



**CHALMERS**  
UNIVERSITY OF TECHNOLOGY

# **Uncertainty and Sensitivity Analysis for Nuclear Reactor Noise Simulations**

Master's Degree thesis

*Master's Thesis in Master Program in Nuclear Science and Technology*

Huaiqian Yi

Department of Physics  
Chalmers University of Technology  
Gothenburg, Sweden 2017  
CTH-NT-330

ISSN 1653-4662



CTH-NT-330

# **Uncertainty and Sensitivity Analysis for Nuclear Reactor Noise Simulations**

Huaiqian Yi

Department of Physics  
CHALMERS UNIVERSITY OF TECHNOLOGY  
Gothenburg, Sweden 2017

# Uncertainty and Sensitivity Analysis for Nuclear Reactor Noise Simulations

HUAIQIAN YI

©HUAIQIAN YI, 2017

Master's Thesis  
CTH-NT-330  
ISSN 1653-4662  
Department of Physics  
Chalmers University of Technology  
SE-412 96 Gothenburg  
Sweden  
E-mail: [huaiqian@student.chalmers.se](mailto:huaiqian@student.chalmers.se)

Chalmers Reproservice  
Gothenburg, Sweden 2017

Uncertainty and Sensitivity Analysis for Nuclear Reactor Noise Simulations  
Master's Thesis in Master Program in Nuclear Science and Technology  
HUIQIAN YI  
Department of Physics  
Chalmers University of Technology

## Abstract

Neutron noise in nuclear reactors is related to the fluctuations of the neutron flux that can occur in stationary operational conditions. These fluctuations may be induced by different types of phenomena such as vibration of reactor components, perturbations of the coolant flow, stochastic aspects of nuclear fissions, etc. Neutron noise carries information about the actual properties of the reactor, and its analysis can help to diagnose anomalies that can evolve over time into more severe issues.

The aim of the thesis is to evaluate the impact of modelling uncertainties on reactor noise simulations. For this purpose, the reactor noise simulator CORE SIM together with a statistical methodology for input uncertainty propagation are used.

A simplified light water reactor with a thermal neutron absorber of variable strength placed in one point of the core, is analyzed. The uncertainties associated to the macroscopic neutron cross-sections of the core and to the neutron absorber, are considered. These uncertainties are assumed to behave as random variables with either a uniform or a normal probability density function. Then random samples can be generated for each type of cross-sections in each point of the core and for the noise source (i.e. the neutron absorber), and be propagated to the CORE SIM outputs. The calculations are performed for both the forward and the adjoint noise, and the results are used for the uncertainty and sensitivity analysis.

The uncertainty analysis shows that the probability density functions of the outputs are close to normal distributions, whether the input uncertainties are normally or uniformly distributed.

The Pearson correlation coefficient is used to quantify the sensitivity of the calculated forward and adjoint noise to the uncertain input parameters. The noise in the core is strongly correlated to the cross-sections taken at the position of the noise source, and to the characteristics of the noise source. In general terms, the most influential macroscopic cross-sections are found to be the thermal fission, thermal capture, and removal ones.

**Keywords:** reactor noise analysis, CORE SIM, statistical code uncertainty propagation, uncertainty and sensitivity analysis, macroscopic cross-section



## **Acknowledgments**

I would first like to express my sincere gratitude and appreciation to my two thesis supervisors Paolo Vinai and Christophe Demazière.

My deepest thanks to Paolo for supporting and guiding me through the entire process of the work and without whose guidance and patience, the thesis wouldn't have been successful. The detailed discussions I had with him, the guiding suggestions he rendered to me, have enlightened me and were of tremendous help in both tackling the problems I faced and writing the final report.

I would also like to express my gratefulness to Christophe Demazière for the discussions which provided me with inspiring ideas and helped to improve the work.

Special thanks to Klas Jaretag for the help with setting up the perfect working environment and bringing up interesting research topics in the conversations we had.

Finally I would like to thank my parents for their support and care throughout the years of my studies, and also my girlfriend who had given me continuous encouragement.



# Table of Contents

<b>1 Introduction .....</b>	<b>1</b>
<b>1.1 Nuclear energy .....</b>	<b>1</b>
<b>1.2 Nuclear reactors and reactor noise.....</b>	<b>2</b>
<b>1.3 Uncertainty and sensitivity analysis .....</b>	<b>4</b>
<b>1.4 Objective and outline of the thesis .....</b>	<b>4</b>
<b>2 CORE SIM and uncertainty and sensitivity analysis.....</b>	<b>7</b>
<b>2.1 The multi-purpose neutronic tool CORE SIM.....</b>	<b>7</b>
2.1.1 Two-group neutron diffusion theory.....	7
2.1.2 Neutron noise equations based on 2-group diffusion theory.....	9
2.1.3 Equations implemented in CORE SIM .....	10
2.1.4 Types of neutron noise sources.....	12
2.1.5 Relationship between the adjoint and forward problems .....	13
2.1.6 Input data for CORE SIM .....	14
2.1.7 Output of CORE SIM .....	16
<b>2.2 Procedure for uncertainty and sensitivity analysis .....</b>	<b>18</b>
<b>2.3 Uncertainty in the input parameters .....</b>	<b>20</b>
<b>2.4 Uncertainty analysis of the code output .....</b>	<b>24</b>
<b>2.5 Statistical measures for sensitivity analysis .....</b>	<b>25</b>
<b>3 Uncertainty analysis .....</b>	<b>27</b>
<b>3.1 Uncertainty of the absorption cross-sections.....</b>	<b>27</b>
<b>3.2 Output uncertainties in the forward problem .....</b>	<b>30</b>
3.2.1 Results from input samples with uniform distributions.....	30
3.2.2 Results from input samples with normal distributions .....	32
3.2.3 Comparison between the uniform and normal cases.....	33
<b>3.3 Output uncertainties in the adjoint problem .....</b>	<b>35</b>
3.3.1 Results from input samples with uniform distributions.....	36

3.3.2 Results from input samples with normal distributions .....	38
3.3.3 Comparison between the uniform and normal cases .....	39
<b>3.4 Comparison between the forward and adjoint calculations .....</b>	<b>40</b>
<b>4 Sensitivity analysis .....</b>	<b>43</b>
<b>4.1 Sensitivity analysis for the forward problem .....</b>	<b>43</b>
4.1.1 Correlations between uncertain input parameters and noise in the same node .....	44
4.1.2 Pearson correlation coefficient between the thermal capture cross-section over level 7 and the noise in a fixed position .....	49
4.1.3 Pearson correlation coefficient between source strength and noise magnitude over level 7 .....	51
<b>4.2 Sensitivity analysis for the adjoint problem .....</b>	<b>52</b>
4.2.1 Correlations between the uncertain input parameters and the noise in the same node .....	52
4.2.2 Pearson correlation coefficient between input parameters and adjoint noise from different nodes .....	57
4.2.3 Pearson correlation coefficient between the source frequency and the phase of the adjoint noise over level 7 .....	62
<b>4.3 Comparison between the forward and adjoint calculations .....</b>	<b>63</b>
<b>5 Summary and conclusions .....</b>	<b>65</b>
<b>Reference .....</b>	<b>67</b>

# Nomenclature

## Symbols:

$E$	Neutron energy [ $kgm^2s^{-2}$ ]
$\omega$	Angular frequency [ $rads^{-1}$ ]
$\mathbf{J}$	Neutron current density vector [ $m^{-2}s^{-1}$ ]
$\phi$	Scalar neutron flux [ $m^{-2}s^{-1}$ ]
$\delta\phi$	Neutron noise [a. u.]
$D$	Diffusion coefficient [m]
$v$	Neutron speed [ $ms^{-1}$ ]
$\beta$	Fraction of delayed neutrons [1]
$\chi$	Fission neutron spectrum [1]
$\nu$	Fission neutron yield [1]
$\lambda$	Decay constant [ $s^{-1}$ ]
$C$	Concentration of the precursors [ $m^{-3}$ ]
$\Sigma_T$	Total macroscopic cross-section [ $m^{-1}$ ]
$\Sigma_a$	Macroscopic absorption cross-section [ $m^{-1}$ ]
$\Sigma_c$	Macroscopic capture cross-section [ $m^{-1}$ ]
$\Sigma_f$	Macroscopic fission cross-section [ $m^{-1}$ ]
$\Sigma_{s0}$	Macroscopic scattering cross-section [ $m^{-1}$ ]
$\Sigma_r$	Macroscopic removal cross-section [ $m^{-1}$ ]
$\mathbf{r}$	Space coordinate
$t$	Time coordinate

## Subscripts:

$g$	Neutron energy group
$g' \rightarrow g$	Neutron scattering from energy group $g'$ to $g$
0	Nominal value
1	Fast neutron group
2	Thermal Neutron group
max	Maximum value
min	Minimum value

## Superscripts:

$p$	Prompt neutrons
$d$	Delayed neutrons
$T$	Transpose of a matrix
$\dagger$	Adjoint notation



# 1 Introduction

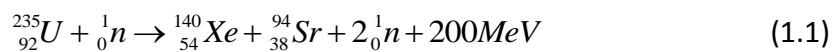
## 1.1 Nuclear energy

Nuclear energy is a type of primary energy that can be used for electricity generation. A large amount of this form of energy can be released from a little amount of material, so large energy to fuel ratio can be achieved. On the other hand, the use of it is associated to a high risk because of the production of strongly radioactive materials.

The first nuclear pile was built by Fermi in 1942. During World War II nuclear energy and technology had a quick and huge development in USA, within the framework of the Manhattan project under the military supervision, for the purpose of the atomic bomb. In 1950s, the focus turned to peaceful and civil use of nuclear energy for generating electricity with controlled chain reactions.

Currently there are over 440 commercial nuclear power reactors operating in 31 countries with 60 more reactors under construction, not including the 245 civil research reactors. The total capacity of nuclear power is over 390,000 MWe and covers 11% of the world's electricity supply [1]. Nuclear power acts as a continuous and reliable base load power, which emits almost no greenhouse gases.

The primary energy comes from splitting heavy nuclei, such as plutonium and uranium. The nucleus consists of nucleons (protons and neutrons), and it is the strong interaction force that holds them together with a very small interacting range. In order to split the nucleus it is necessary to provide an amount of energy equal to the binding energy. In the process of splitting heavy nuclei into lighter nuclei energy will be released in the form of photons and kinetic energy of the fission products. In nuclear reactors, fission is mainly due to neutrons colliding with the uranium-235:



From this fission reaction, on average 2-3 new neutrons are emitted and can be used to induce other fission reactions, so that a self-sustainable chain reaction is possible. However, the produced neutrons are fast neutron with average energy of 2 MeV. At these energies the neutron fission cross-sections of uranium-235 (i.e. the probability that a neutron can induce fission with uranium-235) is much lower than at thermal energies. This means that either a very high concentration of uranium-235 must be available or the neutrons generated in the fission process must be slowed down to thermal energies by moderation.

Most of the current nuclear power reactors are thermal (i.e. based on thermal fissions) and use a moderator.

The quality of the moderator is quantified by the amount of energy that the

neutron will lose per elastic scattering with the moderator, by the probability of elastic scattering, and by the probability of absorption. Higher amount of energy lost, larger probability of scattering and lower probability of absorption defines a good moderator. Water and graphite are usually chosen as neutron moderator because of the low probability of capturing neutrons. However, the graphite has some unsatisfying properties, so the most used moderator is water.

With the combination of appropriate enrichment of the uranium fuel and the right volume of moderator, a self-sustaining and steady chain reaction can be obtained in a nuclear reactor for electricity production.

## 1.2 Nuclear reactors and reactor noise

The reactor core is a bounded region contained in the reactor pressure vessel, it contains the fuel assemblies and moderator. It is the place where neutron multiplication and the chain reactions take place. With an ongoing chain reaction, heat can be continuously generated and extracted by the coolant. The most common commercial reactors are Light Water Reactors (LWRs), where light water is used as neutron moderator and as coolant. Two main designs of LWRs are available: Pressurized Water Reactor (PWR) and Boiling water Reactor (BWR) as shown in Fig. 1.1. The PWR sends the heated water from the core to the steam generator for steam production, while BWR produces steam directly in the core.

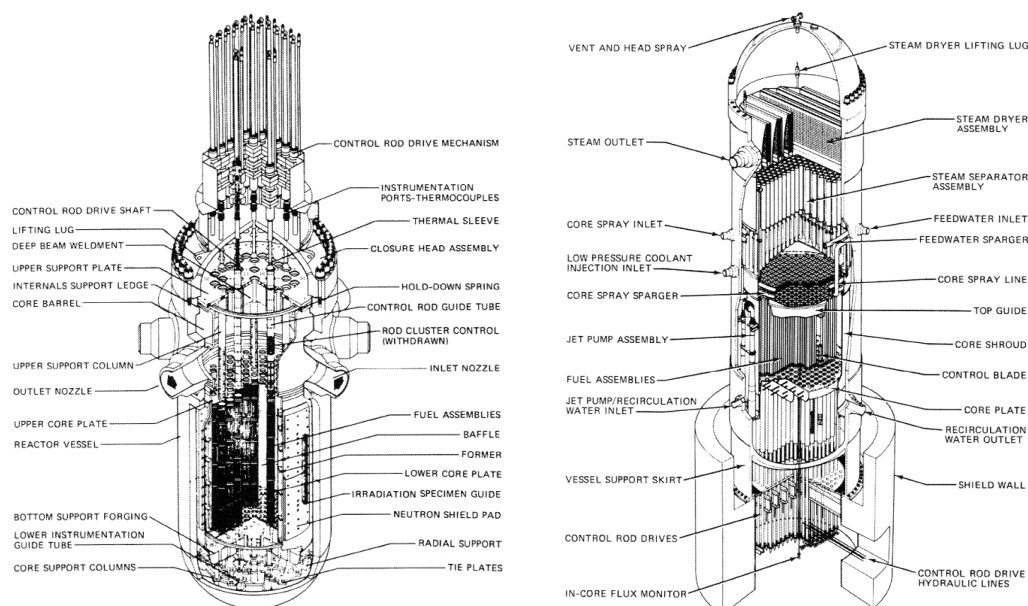


Figure 1.1 Internal structure of a PWR (left) and a BWR (right) [2].

The reactor core consists of fuel assemblies. Several fuel rods, which are made from  $\text{UO}_2$  pellets, are compiled into a fuel assembly. These fuel assemblies are located in the core and they contain different amounts of uranium-235 and additional materials so that the distribution of neutron density field in the core is as flat as possible and that hot spots are avoided. The ultimate aim of core control is to keep the

reactor in critical condition for the entire operating time. For such kind of purpose, some measures are taken. For instance by adding burnable absorbers in the fuel elements allows to compensate for the change in the fuel along time (in fact uranium-235 is consumed along the operations). In normal operations, small deviations from the critical state can be adjusted by tuning different plant parameters and systems. The fissions and so the reactor power can be adjusted by inserting or withdrawing control rods or by altering the concentration of boron (which is a neutron absorber) in the water flowing through the reactor.

Considering the complexity and heterogeneities of a nuclear core, it can be a difficult task to predict the behavior of the neutron density distribution. However, through the usage of cross-sections, the behavior of the core can be modelled rather accurately. The microscopic cross-section is an “effective area” that quantifies the probability of a certain reaction given a target nucleus and an incident particle. In case of nuclear reactors, these cross-sections are defined for neutrons. A more useful parameter is the macroscopic cross sections which takes into account a target containing more nuclei, even different types of nuclei. The macroscopic cross-section has a unit of  $cm^{-1}$  and has a physical meaning that represents the probability of interaction per unit path length. Thus the types of interaction that the neutrons could have with the target materials in the core can be represented and classified as:

- The absorption cross-section: this includes both capture of the neutrons that results in forming a heavier nuclei and capture of neutrons that will induce fission of the fuel.
- The fission cross section: quantifies the probability that fission will be induced
- The scattering cross section: the probability that the neutron will be scattered when colliding with the target nuclei rather than absorbed.

Once the cross-sections have been properly defined and calculated, the neutron flux at the core level can be calculated using for instance a two group neutron diffusion approximation. This approach is described in more details in the next chapter.

As mentioned above, a steady and stable neutron flux in the reactor is needed for producing electricity in a stationary manner. However, fluctuations of the neutron flux are inevitable and exist in all operating stages of a nuclear reactor.

At low power, the “zero power reactor noise” dominates. The existence of such noise is not due to the change in material properties of the core but rather the stochastic nature of nuclear processes. The random distribution of the neutron distribution in reactors operating at low power arises from the randomness of nuclear processes such as how far a neutron will travel or for how long time it will exist before it interacts with other atoms, what kind of reaction will arise from neutron-atom interactions and if a fission event is induced, how many more neutrons will be emitted. The “zero power reactor” noise dominates over the “power reactor noise” in low power (low level of static flux) as the variance of the former is proportional to the static (mean) neutron flux while the variance of the latter is proportional to the square of the static neutron flux [3].

In reactors which is operating at a high power level, with also a high level of the static neutron flux, the “power reactor noise” dominates. In such systems, the change in material properties or reactor conditions will be the driving force for perturbations in the static neutron flux. These changes can be, for instance, fluctuations related to: the temperature of the fuel or the moderator; the pressure or the flow of the coolant; mechanical vibrations of internals such as fuel rods or control rod. All these perturbations can cause the macroscopic cross-sections of the core and so the neutron flux to fluctuate.

The analysis of the zero power reactor noise allows to extract some important information about the nuclear properties of the system such as cross-sections and reactivity. The analysis of the power reactor noise can help to identify issues and malfunctions of the reactor core, before the situation can escalate. Therefore there has been an interest in the development and application of noise analysis techniques for diagnostic purposes [4], [5], [6].

### **1.3 Uncertainty and sensitivity analysis**

In the nuclear industry there is a high demand for realistic simulations with reliable confidence levels, for operating reactors with sufficiently large safety margins.

Although high fidelity is an important goal for modelling of nuclear reactors, the calculated results always deviate from the real solutions. These deviations are due to a number of uncertainties that can arise from the basic nuclear data, the boundary and initial conditions, approximations in the computational models, etc. Then the quantification of the impact of the uncertainties on the calculated results are necessary.

Sensitivity analysis is also another significant aspect. Computer codes process a number of input parameters used to describe the system and provides output results. Sensitivity analysis can provide information about the dependency of the outputs on the model inputs, and help to discriminate the most important input modelling parameters. As a result, a better understanding of models can be achieved and possible improvements can be identified.

### **1.4 Objective and outline of the thesis**

The objective of this thesis work is to investigate the impact of input uncertainties on reactor noise simulations for a localized perturbation in the core. For this purpose, the reactor noise simulator CORE SIM is used. The input uncertainties are related to the macroscopic cross-sections of the core, and to the parameters that describe the neutron noise source. The uncertainty and sensitivity analysis is based on a statistical methodology, and it is performed for both the forward and the adjoint neutron noise calculation.

The structure of the thesis is as follows. In chapter 2, the methodology used in the work is described. In chapter 3, the results from the uncertainty analysis of the forward and adjoint calculations are discussed. In chapter 4, the results of the sensitivity analysis for the forward and adjoint calculations are presented. In chapter 5, concluding remarks are provided.



## 2 CORE SIM and uncertainty and sensitivity analysis

In this chapter the methodology followed in the work is described. The reactor noise simulator CORE SIM and the basic equations implemented in the tool are introduced in section 2.1. The procedure for the uncertainty and sensitivity analysis is discussed in section 2.2. The uncertainties associated to the input parameters are described in section 2.3. The approach for the analysis of the output is explained in sections 2.4 and 2.5.

### 2.1 The multi-purpose neutronic tool CORE SIM

CORE SIM is a neutronic tool that can be used for neutronic simulations of both critical reactors and subcritical systems with an external neutron source. The static neutron flux and the first order neutron noise together with their adjoint functions can be calculated. Since the present study is on a LWR-type of a reactor core, the discussion is focused only on critical systems.

#### 2.1.1 Two-group neutron diffusion theory

The calculation of CORE SIM relies on the 2-group diffusion theory and one group of delayed neutrons. The multi-group diffusion equation can be derived from the energy-dependent transport equation by using a few approximations as given below.

A relationship can be established between the current density vector and the scalar neutron flux using the Fick's law which states that:

$$\mathbf{J}(\mathbf{r}, E, t) = -D(\mathbf{r}, E, t) \bar{\nabla} \phi(\mathbf{r}, E, t). \quad (2.1)$$

The diffusion coefficient  $D(\mathbf{r}, E)$  is usually expressed as:

$$D(\mathbf{r}, E, t) = \frac{1}{3\Sigma_{tr}(\mathbf{r}, E, t)}. \quad (2.2)$$

In this expression the macroscopic transport cross-section is used for the diffusion coefficient, so the anisotropy scattering can be represented to some extent and some features of the transport equation can be recovered.

The energy dependence of the diffusion equation is handled using the multi-group formalism where the range of possible neutron energy is divided into  $G$  energy bins as:

$$[E_{\min}; E_{\max}] = \bigcup_{g=G}^1 [E_g; E_{g-1}], \quad (2.3)$$

where the first group ( $g = 1$ ) has the highest energy neutrons and the last group ( $g = G$ ) represents neutrons with the lowest energy.

When dealing with non-steady-state systems, the fission source term should be handled with care as some neutrons are produced within  $10^{-7}$  s and are referred to as prompt neutrons, while delayed neutrons appear after a  $\beta^-$  decay of some fission fragments (precursors of delayed neutrons). The delayed neutrons are modelled by tracking the precursors. In the case of only one family of precursors, three additional parameters are defined as: the fraction of delayed neutrons  $\beta$ ; the decay constant of the precursors  $\lambda$ ; and the space- and time-dependent concentration of the precursors  $C(\mathbf{r}, t)$ .

As a result, the time-dependent diffusion equation can be expressed as [7]:

$$\begin{aligned} \frac{1}{v_g} \frac{\partial}{\partial t} \phi_g(\mathbf{r}, t) = & \bar{\nabla} \cdot [D_g(\mathbf{r}, t) \bar{\nabla} \phi_g(\mathbf{r}, t)] + \sum_{g'=1}^G \Sigma_{s0, g' \rightarrow g}(\mathbf{r}, t) \phi_{g'}(\mathbf{r}, t) \\ & + (1 - \beta) \chi_g^p \sum_{g'=1}^G \nu \Sigma_{f, g'}(\mathbf{r}, t) \phi_{g'}(\mathbf{r}, t) \\ & + \lambda \chi_g^d C(\mathbf{r}, t) - \Sigma_{T, g} \phi_g(\mathbf{r}, t) \end{aligned} \quad (2.4)$$

with  $\chi_g^p$  and  $\chi_g^d$  both fulfilling

$$\sum_{g=1}^G \chi_g^p = \sum_{g=1}^G \chi_g^d = 1 \quad (2.5)$$

and representing the relative contribution of the prompt and delayed neutrons in the energy group  $g$  respectively. An additional equation is required for the concentration of the precursors, i.e.:

$$\frac{\partial}{\partial t} C(\mathbf{r}, t) = \beta \sum_{g=1}^G \nu \Sigma_{f, g}(\mathbf{r}, t) - \lambda C(\mathbf{r}, t). \quad (2.6)$$

CORE SIM is based on 2-group diffusion theory. Then, Eqs. (2.4) and (2.6) can be simplified as follows:

$$\begin{aligned} \frac{1}{v_1} \frac{\partial}{\partial t} \phi_1(\mathbf{r}, t) = & \bar{\nabla} \cdot [D_{1,0} \bar{\nabla} \phi_1(\mathbf{r}, t)] + [(1 - \beta) \nu \Sigma_{f,1}(\mathbf{r}, t) - \Sigma_{a,1}(\mathbf{r}, t) \\ & - \Sigma_r(\mathbf{r}, t)] \phi_1(\mathbf{r}, t) + (1 - \beta) \nu \Sigma_{f,2}(\mathbf{r}, t) \phi_2(\mathbf{r}, t) + \lambda C(\mathbf{r}, t) \end{aligned} \quad (2.7)$$

$$\begin{aligned} \frac{1}{v_2} \frac{\partial}{\partial t} \phi_2(\mathbf{r}, t) = & \bar{\nabla} \cdot [D_{2,0} \bar{\nabla} \phi_2(\mathbf{r}, t)] + \Sigma_r(\mathbf{r}, t) \phi_1(\mathbf{r}, t) \\ & - \Sigma_{a,2}(\mathbf{r}, t) \phi_2(\mathbf{r}, t) \end{aligned} \quad (2.8)$$

$$\frac{\partial}{\partial t} C(\mathbf{r}, t) = \beta \nu \Sigma_{f,1}(\mathbf{r}, t) + \beta \nu \Sigma_{f,2}(\mathbf{r}, t) - \lambda C(\mathbf{r}, t). \quad (2.9)$$

with the removal cross-section defined as:

$$\Sigma_r(\mathbf{r}, t) = \Sigma_{s,0,1 \rightarrow 2}(\mathbf{r}, t) - \frac{\Sigma_{s,0,2 \rightarrow 1}(\mathbf{r}, t) \phi_2(\mathbf{r}, t)}{\phi_1(\mathbf{r}, t)} \quad (2.10)$$

In the above expressions,  $\phi_1$  is the fast neutron flux and  $\phi_2$  is the thermal neutron flux. It is assumed that both the prompt and delayed neutron are produced only as fast neutrons and thus only contributing to the fast group. The diffusion coefficients are considered to be time-independent, as it decreases the computational burden without relevant differences in the results [8].

### 2.1.2 Neutron noise equations based on 2-group diffusion theory

CORE SIM is designed to treat the case of stationary perturbations. The equations for the fluctuations of the neutron flux (i.e. the neutron noise) are derived from linear perturbation theory.

In Eqs. (2.7) to (2.9), the generic time-dependent quantity  $X(\mathbf{r}, t)$  can be split into two parts. The first part is the mean value which corresponds to the steady state condition or to the critical configuration of the system, and thus it is independent of time and is denoted as  $X_0(\mathbf{r})$ . The second part is the fluctuation around their mean value and this fluctuation varies with time, and it is denoted as  $\delta X(\mathbf{r}, t)$ . Thus each time dependent quantity can be written as:

$$X(\mathbf{r}, t) = X_0(\mathbf{r}) + \delta X(\mathbf{r}, t). \quad (2.11)$$

The time-dependent quantities, as can be seen in Eqs. (2.7) through (2.9), can be the macroscopic cross-sections in both groups, the neutron flux and the concentration of the precursors.

The derivation of the 2-group equations for the neutron noise consists of the following steps. First, Eq. (2.11) is substituted in Eqs. (2.7)-(2.9) for all the time – dependent quantities. Second, the second order terms (in the form  $\delta X(\mathbf{r}, t) \cdot \delta Y(\mathbf{r}, t)$ ) are neglected, i.e. linear theory is applied. Third, the time-independent equations,

$$\begin{aligned} \bar{\nabla} \cdot [D_{1,0} \bar{\nabla} \phi_{1,0}(\mathbf{r})] + [(1 - \beta) \nu \Sigma_{f,1,0}(\mathbf{r}) - \Sigma_{a,1,0}(\mathbf{r}) \\ - \Sigma_{r,0}(\mathbf{r})] \phi_{1,0}(\mathbf{r}) + (1 - \beta) \nu \Sigma_{f,2,0}(\mathbf{r}) \phi_{2,0}(\mathbf{r}) = 0 \end{aligned} \quad (2.12)$$

$$\bar{\nabla} \cdot [D_{2,0} \bar{\nabla} \phi_{2,0}(\mathbf{r})] + \Sigma_{r,0}(\mathbf{r}) \phi_{1,0}(\mathbf{r}) - \Sigma_{a,2,0}(\mathbf{r}) \phi_{2,0}(\mathbf{r}) = 0 \quad (2.13)$$

are subtracted from the time-dependent equations. Fourth, a Fourier transform is performed in angular frequency ( $\omega = 2\pi f$ ) on each and every term of the equation

and the following property is used:

$$\mathcal{F}\left(\frac{df(x)}{dx}\right) = (i\omega)\mathcal{F}(f(x)). \quad (2.14)$$

Fifth, the equation describing the concentration of precursors is eliminated. Finally the equations describing the dynamic behavior is obtained:

$$\begin{aligned} & \nabla \cdot D_{1,0} \nabla \cdot \delta\phi_1(\mathbf{r}, \omega) - \left[ \Sigma_{a,1,0}(\mathbf{r}) + \frac{i\omega}{v_1} + \Sigma_{r,0}(\mathbf{r}) \right] \cdot \delta\phi_1(\mathbf{r}, \omega) \\ & + \frac{\nu\Sigma_{f,1,0}(\mathbf{r})}{k_{eff}} \left( 1 - \frac{i\omega\beta}{i\omega + \lambda} \right) \cdot \delta\phi_1(\mathbf{r}, \omega) + \frac{\nu\Sigma_{f,2,0}(\mathbf{r})}{k_{eff}} \left( 1 - \frac{i\omega\beta}{i\omega + \lambda} \right) \cdot \delta\phi_2(\mathbf{r}, \omega) \quad (2.15) \\ & = \phi_{1,0}(\mathbf{r}) \delta\Sigma_r(\mathbf{r}, \omega) + \phi_{1,0}(\mathbf{r}) \delta\Sigma_{a,1}(\mathbf{r}, \omega) - \phi_{1,0}(\mathbf{r}) \left( 1 - \frac{i\omega\beta}{i\omega + \lambda} \right) \delta\nu\Sigma_{f,1}(\mathbf{r}, \omega) \end{aligned}$$

$$\begin{aligned} & \nabla \cdot D_{2,0} \nabla \cdot \delta\phi_2(\mathbf{r}, \omega) - \left[ \Sigma_{a,2,0}(\mathbf{r}) + \frac{i\omega}{v_2} \right] \cdot \delta\phi_2(\mathbf{r}, \omega) + \Sigma_{r,0}(\mathbf{r}) \cdot \delta\phi_1(\mathbf{r}, \omega) \quad (2.16) \\ & = -\phi_{1,0} \delta\Sigma_r(\mathbf{r}, \omega) + \phi_{2,0} \delta\Sigma_{a,2}(\mathbf{r}, \omega) \end{aligned}$$

The Fourier transform of any quantity  $\delta X(\mathbf{r}, t)$  is obtained according to:

$$\delta X(\mathbf{r}, \omega) = \int_{-\infty}^{\infty} \delta X(\mathbf{r}, t) e^{-i\omega t} dt \quad (2.17)$$

### 2.1.3 Equations implemented in CORE SIM

The time-independent equation given by Eq. (2.12)-(2.13) will have solution only if the system is critical. The system is critical if the material and geometry properties are such that a perfect neutron balance in the system is obtained, and thus the behavior of the neutron flux is time-independent with  $k_{eff} = 1$ . If the system is not critical (i.e.  $k_{eff} \neq 1$ ), a steady state solution can still be obtained by re-normalizing the fission source terms by a factor  $k_m$ . The effective multiplication factor  $k_{eff}$  is the largest eigenvalue. This eigenvalue is associated to the eigenfunctions that have the same positive sign throughout the core and correspond to the static fluxes of the system, i.e.  $\phi_{1,0}(\mathbf{r})$  and  $\phi_{2,0}(\mathbf{r})$ . The steady state conditions thus solved in CORE SIM is the following eigenvalue equations [8]:

$$\left[ \nabla \cdot \overline{\overline{D}}(\mathbf{r}) \nabla + \overline{\overline{\Sigma}}_{sta}(\mathbf{r}) \right] \times \begin{bmatrix} \phi_{1,m}(\mathbf{r}) \\ \phi_{2,m}(\mathbf{r}) \end{bmatrix} = \frac{1}{k_m} \overline{\overline{F}}(\mathbf{r}) \times \begin{bmatrix} \phi_{1,m}(\mathbf{r}) \\ \phi_{2,m}(\mathbf{r}) \end{bmatrix} \quad (2.18)$$

with

$$\overline{\overline{D}}(\mathbf{r}) = \begin{bmatrix} D_{1,0}(\mathbf{r}) & 0 \\ 0 & D_{2,0}(\mathbf{r}) \end{bmatrix}, \quad (2.19)$$

$$\bar{\Sigma}_{sta}(\mathbf{r}) = \begin{bmatrix} -\Sigma_{a,1,0}(\mathbf{r}) - \Sigma_r(\mathbf{r}) & 0 \\ \Sigma_r(\mathbf{r}) & -\Sigma_{a,2,0}(\mathbf{r}) \end{bmatrix} \quad (2.20)$$

and

$$\bar{F}(\mathbf{r}) = \begin{bmatrix} -\nu\Sigma_{f,1,0}(\mathbf{r}) & -\nu\Sigma_{f,1,0}(\mathbf{r}) \\ 0 & 0 \end{bmatrix}. \quad (2.21)$$

The dynamic equations (2.15) and (2.16) are derived assuming that the system is critical. However, when the system is not critical the dynamic equations can also be obtained by renormalizing the macroscopic fission cross-sections with  $k_{eff}$ . After renormalization, the dynamic equations solved for critical systems in CORE SIM is thus, written in a matrix form:

$$\begin{aligned} & \left[ \nabla \cdot \bar{D}(\mathbf{r}) \nabla + \bar{\Sigma}_{dyn}^{crit}(\mathbf{r}, \omega) \right] \times \begin{bmatrix} \delta\phi_1(\mathbf{r}, \omega) \\ \delta\phi_2(\mathbf{r}, \omega) \end{bmatrix} \\ & = \bar{\phi}_r(\mathbf{r}) \delta\Sigma_r(\mathbf{r}, \omega) + \bar{\phi}_a(\mathbf{r}) \begin{bmatrix} \delta\Sigma_{a,1}(\mathbf{r}, \omega) \\ \delta\Sigma_{a,2}(\mathbf{r}, \omega) \end{bmatrix} + \bar{\phi}_f(\mathbf{r}, \omega) \begin{bmatrix} \delta\nu\Sigma_{f,1}(\mathbf{r}, \omega) \\ \delta\nu\Sigma_{f,2}(\mathbf{r}, \omega) \end{bmatrix} \end{aligned} \quad (2.22)$$

with

$$\bar{D}(\mathbf{r}) = \begin{bmatrix} D_{1,0}(\mathbf{r}) & 0 \\ 0 & D_{2,0}(\mathbf{r}) \end{bmatrix}, \quad (2.23)$$

$$\bar{\Sigma}_{dyn}^{crit}(\mathbf{r}, \omega) = \begin{bmatrix} -\Sigma_1^{crit}(\mathbf{r}, \omega) & \frac{\nu\Sigma_{f,2,0}(\mathbf{r})}{k_{eff}} \left( 1 - \frac{i\omega\beta}{i\omega + \lambda} \right) \\ \Sigma_{r,0}(\mathbf{r}) & -\Sigma_{a,2,0}(\mathbf{r}) + \frac{i\omega}{\nu_2} \end{bmatrix}, \quad (2.24)$$

$$\Sigma_1^{crit}(\mathbf{r}, \omega) = \Sigma_{a,2,0}(\mathbf{r}) + \frac{i\omega}{\nu_1} + \Sigma_{r,0}(\mathbf{r}) - \frac{\nu\Sigma_{f,1,0}(\mathbf{r})}{k_{eff}} \left( 1 - \frac{i\omega\beta}{i\omega + \lambda} \right), \quad (2.25)$$

$$\bar{\phi}_r(\mathbf{r}) = \begin{bmatrix} \phi_{1,0}(\mathbf{r}) \\ -\phi_{1,0}(\mathbf{r}) \end{bmatrix}, \quad (2.26)$$

$$\bar{\phi}_a(\mathbf{r}) = \begin{bmatrix} \phi_{1,0}(\mathbf{r}) & 0 \\ 0 & \phi_{2,0}(\mathbf{r}) \end{bmatrix} \quad (2.27)$$

and

$$\bar{\phi}_f(\mathbf{r}, \omega) = \begin{bmatrix} -\frac{\phi_{1,0}(\mathbf{r})}{k_{eff}} \left( 1 - \frac{i\omega\beta}{i\omega + \lambda} \right) & -\frac{\phi_{2,0}(\mathbf{r})}{k_{eff}} \left( 1 - \frac{i\omega\beta}{i\omega + \lambda} \right) \\ 0 & 0 \end{bmatrix}. \quad (2.28)$$

In the current work, the adjoint calculations are also evaluated. In fact the adjoint

problem is also of interest because of some useful properties [8]. The inner product between two space-dependent flux functions  $\bar{\varphi}(\mathbf{r}) = [\varphi_1(\mathbf{r}) \varphi_2(\mathbf{r})]^T$  and  $\bar{\psi}(\mathbf{r}) = [\psi_1(\mathbf{r}) \psi_2(\mathbf{r})]^T$  is defined as:

$$(\bar{\psi}, \bar{\varphi}) = \int_V \bar{\psi}^T(\mathbf{r}) \cdot \bar{\varphi}(\mathbf{r}) d\mathbf{r} \quad (2.29)$$

The operator  $\bar{L}^\dagger$  is the adjoint of the operator  $\bar{L}$  if it satisfies the following expression [9]:

$$(\bar{\phi}^\dagger, \bar{L} \times \bar{\phi}) = (\bar{L}^\dagger \times \bar{\phi}^\dagger, \bar{\phi}). \quad (2.30)$$

Then, the adjoint noise problem associated with the forward noise problem is given by:

$$\left[ \nabla \cdot \bar{D}(\mathbf{r}) \nabla + \bar{\Sigma}_{dyn}^{crit\dagger}(\mathbf{r}, \omega) \right] \times \begin{bmatrix} \delta\phi_1^\dagger(\mathbf{r}, \omega) \\ \delta\phi_2^\dagger(\mathbf{r}, \omega) \end{bmatrix} = - \begin{bmatrix} \delta S_1^\dagger(\mathbf{r}, \omega) \\ \delta S_2^\dagger(\mathbf{r}, \omega) \end{bmatrix} \quad (2.31)$$

where

$$\bar{\Sigma}_{dyn}^{crit\dagger}(\mathbf{r}, \omega) = \bar{\Sigma}_{dyn}^{critT}(\mathbf{r}, \omega). \quad (2.32)$$

The superscript  $T$  indicates the transpose of the matrix operator.

In brief, one CORE SIM calculation in a critical system provides the solution of the eigenvalue equations given by Eq. (2.18). Once the eigenvalue ( $k_0 = k_{eff}$ ) and the eigenfunctions ( $\phi_{1,0}(\mathbf{r})$  and  $\phi_{2,0}(\mathbf{r})$ ) for the fundamental mode have been determined, then they are used for the forward noise calculation based on Eq. (2.22). The same procedure is applied to the adjoint case.

## 2.1.4 Types of neutron noise sources

In Eq. (2.22) the fluctuation of the neutron flux (i.e., the neutron noise) may be induced by the fluctuation of the absorption cross section ( $\delta\Sigma_a(\mathbf{r}, \omega)$ ), the fluctuation of the fission cross-section ( $\delta\nu\Sigma_f(\mathbf{r}, \omega)$ ) and the fluctuation of the removal cross-section ( $\delta\Sigma_r(\mathbf{r}, \omega)$ ). As mentioned in section 1.2, the fluctuations of the cross-sections can be due to different types of perturbations, such as an absorber of variable strength in the core, a vibrating control rod, or oscillations of the property of the moderator/coolant.

In this thesis the neutron noise induced by an absorber of variable strength is studied. This kind of a perturbation is localized, i.e. its position does not vary. The scenario can be then modelled with Eq. (2.22), where the noise source is specified in terms of only  $\delta\Sigma_a(\mathbf{r}, \omega)$  (and where  $\delta\nu\Sigma_f(\mathbf{r}, \omega)$  and  $\delta\Sigma_r(\mathbf{r}, \omega)$  are set equal to zero).

### 2.1.5 Relationship between the adjoint and forward problems

The forward noise equation (2.22) can be written in a compact form as:

$$\mathbf{L}\delta\phi = \delta S \quad (2.33)$$

A localized neutron noise source in  $\mathbf{r}_s$  is considered. The type of source is an absorber of variable strength and it can be modelled with fluctuations in the thermal absorption cross-section. Then the source in the forward problem can be defined as follows:

$$\delta S(\mathbf{r}, \omega) = \begin{bmatrix} 0 \\ \gamma_2 \delta(\mathbf{r} - \mathbf{r}_s) \end{bmatrix} \quad (2.34)$$

where

$$\gamma_2 = \phi_{2,0}(\mathbf{r}) \delta \Sigma_{a,2,0}(\mathbf{r}). \quad (2.35)$$

The adjoint problem solved in CORE SIM is given by Eq. (2.31) which can also be written in a compact form as:

$$\mathbf{L}^\dagger \delta\phi^\dagger = \delta S^\dagger \quad (2.36)$$

If the adjoint noise source is defined as a point-like source in the thermal group, then it can be written as:

$$\delta S^\dagger = \begin{bmatrix} 0 \\ -\gamma_4 \delta(\mathbf{r} - \mathbf{r}_0) \end{bmatrix} \quad (2.37)$$

The associated adjoint noise is denoted as:

$$\delta\phi^\dagger = \begin{bmatrix} \delta\phi_{2,1}^\dagger(\mathbf{r}, \mathbf{r}_0, \omega) \\ \delta\phi_{2,2}^\dagger(\mathbf{r}, \mathbf{r}_0, \omega) \end{bmatrix}. \quad (2.38)$$

In Eq. (2.38) the first subscript of the adjoint neutron noise indicates the energy group in which the adjoint noise source is defined, while the second index indicates the energy group of the adjoint noise.

Similarly, a point-like adjoint source can be chosen in the fast group as:

$$\delta S^\dagger = \begin{bmatrix} -\gamma_3 \delta(\mathbf{r} - \mathbf{r}_0) \\ 0 \end{bmatrix} \quad (2.39)$$

The corresponding adjoint noise can then be expressed as:

$$\delta\phi^\dagger = \begin{bmatrix} \delta\phi_{1,1}^\dagger(\mathbf{r}, \mathbf{r}_0, \omega) \\ \delta\phi_{1,2}^\dagger(\mathbf{r}, \mathbf{r}_0, \omega) \end{bmatrix}. \quad (2.40)$$

Taking the case where the source of the adjoint problem is in the thermal group as example, the relation between the forward thermal noise and the adjoint noise can be derived.

From the definition of adjoint operator, the following relationship can be written:

$$(\delta\phi^\dagger, \delta S) = (\delta S^\dagger, \delta\phi). \quad (2.41)$$

The latter can be given in an integral form as:

$$\int \begin{bmatrix} \delta\phi_{2,1}^\dagger(\mathbf{r}, \mathbf{r}_0, \omega) \\ \delta\phi_{2,2}^\dagger(\mathbf{r}, \mathbf{r}_0, \omega) \end{bmatrix} \cdot \begin{bmatrix} 0 \\ \gamma_2 \delta(\mathbf{r} - \mathbf{r}_s) \end{bmatrix} dr = \int \begin{bmatrix} \delta\phi_1(\mathbf{r}, \mathbf{r}_s, \omega) \\ \delta\phi_2(\mathbf{r}, \mathbf{r}_s, \omega) \end{bmatrix} \cdot \begin{bmatrix} 0 \\ -\gamma_4 \delta(\mathbf{r} - \mathbf{r}_0) \end{bmatrix} dr \quad (2.42)$$

Thus:

$$\gamma_2 \delta\phi_{2,2}^\dagger(\mathbf{r}_s, \mathbf{r}_0, \omega) = -\gamma_4 \delta\phi_2(\mathbf{r}_0, \mathbf{r}_s, \omega) \quad (2.43)$$

Inserting Eq. (2.35) into Eq. (2.43), and considering that the source strength of the forward and adjoint problem are defined such that  $\delta\Sigma_{a,2,0}(\bar{r}_s) = \gamma_4$ , one finally obtains:

$$\phi_{2,0}(\mathbf{r}_s) \delta\phi_{2,2}^\dagger(\mathbf{r}_s, \mathbf{r}_0, \omega) = -\delta\phi_2(\mathbf{r}_0, \mathbf{r}_s, \omega) \quad (2.44)$$

A similar relation between the forward fast noise and the adjoint noise can be derived:

$$\phi_{2,0}(\mathbf{r}_s) \delta\phi_{1,2}^\dagger(\mathbf{r}_s, \mathbf{r}_0, \omega) = -\delta\phi_1(\mathbf{r}_0, \mathbf{r}_s, \omega) \quad (2.45)$$

When the noise source in the forward problem is due to the fluctuation of the thermal absorption cross-section, the adjoint noise of interest is actually only the thermal adjoint noise, but with the adjoint source either in the fast or in the thermal group.

### 2.1.6 Input data for CORE SIM

The input parameters needed in Eq. (2.22), and also in CORE SIM, are the material data (static macroscopic cross-sections and the diffusion coefficients), the kinetic data, and the perturbations of the macroscopic cross-sections which are the source of the neutron noise.

In CORE SIM, a three dimensional system can be modelled. The system is discretized into a number of equal computational nodes in the Cartesian coordinate system. The equations implemented in CORE SIM are solved for each of the nodes. These equations are spatially averaged with respect to these nodes, and the following node averaged quantities are used:

$$\phi_{g,n}(t) = \frac{1}{V_n} \int_{V_n} \phi_g(\mathbf{r}, t) dr \quad (2.46)$$

$$\Sigma_{X,n} = \frac{\frac{1}{V_n} \int_{V_n} \Sigma_{X,n}(\mathbf{r}, t) \phi_g(\mathbf{r}, t) dr}{\phi_{g,n}(t)} \quad (2.47)$$

with  $V_n$  being the volume of node  $n$  and  $\Sigma_{X,n}$  representing the macroscopic

cross-sections in the node  $n$ . By averaging the macroscopic cross-sections in the way given in Eq. (2.47), the actual reaction rates in each node are preserved.

The nodes are rectangular boxes; the overall nodalization is shown in Fig. 2.1(a) and the nodes of any axial level of the core is presented in Fig 2.1(b).

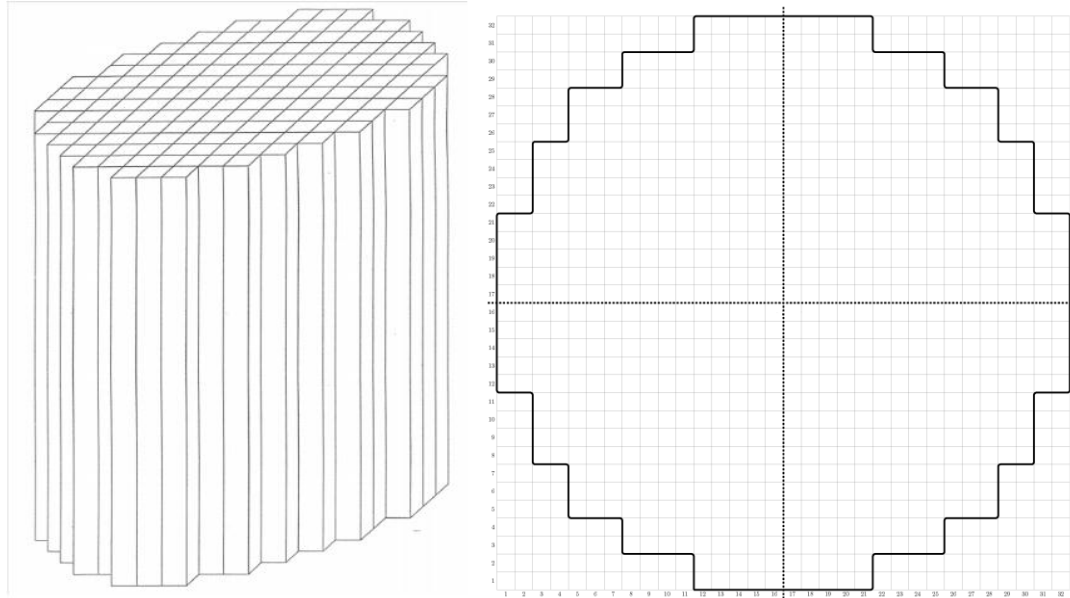


Figure 2.1 (a) A schematic drawing of the discretized core (left), (b) the node on a level of the discretized core, bounded within the black lines which is the boundary of the core

In the thesis work, a simplified LWR core is considered. In particular, the core is homogeneous in terms of material properties, and is surrounded with no reflector.

The core is discretized into 27 levels along the axial direction ( $z$ ); in the ( $x$ - $y$ ) plane, each level includes 800 nodes. Thus the total number of nodes is 21600. Three input values are required in CORE SIM to define the size of the nodes. These values are saved in the input file named “GEOM\_data.mat”. The value used in this work, together with the descriptions are listed in Table 2.1.

Table 2.1 The values used that defines the size of each node used for computation.

Variable name	Description of the variable	Value used [cm]
DX	The length of a node in the x-direction	15.3750
DY	The length of a node in the y-direction	15.3750
DZ	The length of a node in the z-direction	14.7200

According to the node size given above, the core has a diameter of 4.92 m and a height 3.9744 m, which is typical of a LWR.

The reference values for the macroscopic cross-sections data are listed in Table 2.2.

Table 2.2 the material data used in the static and dynamic calculations in case of a bare reactor near to criticality.

$D_{1,0}$	$D_{2,0}$	$\Sigma_{a,1,0}$	$\Sigma_{a,2,0}$	$\Sigma_{r,0}$	$\nu\Sigma_{f,1,0}$	$\nu\Sigma_{f,2,0}$
(cm)	(cm)	(cm <sup>-1</sup> )				
1.8002	0.4338	0.0073	0.0574	0.0131	0.0038	0.0748

The values of the macroscopic cross-sections given in Table 2.2 are assigned to all the nodes of the core, because the core is assumed to be homogeneous. Each node can be identified by a triplet of indexes  $(I, J, K)$ , where  $I$ ,  $J$  and  $K$  refer to the x-, y- and z-directions respectively, so the set of cross-sections assigned to a specific node can be identified by the same triplet of indexes.

The neutron noise source for an absorber of variable strength is determined by assigning a position (i.e. a node given in terms of a triplet of indexes  $(I, J, K)$ ), an amplitude for the variation of the absorption cross-section, and a frequency for the fluctuation of the perturbation. In the current work, the source is located at position (16, 16, 7), has a strength  $\delta\Sigma_{a,2,0} = 1 \text{ cm}^{-1}$  and a frequency equal to 1 Hz.

The nuclear kinetic data needed for the simulation includes the effective fraction of the delayed neutrons  $\beta$ , the decay constant of the neutron precursors  $\lambda$ , and the average neutron speed in the fast and thermal group respectively. The values used in the work are given in Table. 2.3.

Table 2.3 The kinetic data used in dynamic calculations.

$v_1$	$v_2$	$\beta$	$\lambda$
(cm s <sup>-1</sup> )	(cm s <sup>-1</sup> )	(pcm)	(s <sup>-1</sup> )
$1.77746 \times 10^7$	389659	564.06	0.0847

The adjoint calculation also requires static macroscopic cross-sections, kinetic data, and the definition of a source. In order to fulfill the relationship given in Eq. (2.44) and (2.45) for the forward and adjoint noise, the same set of input data is used for the two cases.

### 2.1.7 Output of CORE SIM

Since the calculation made in CORE SIM is in the frequency domain, the results for both the forward and adjoint problem are complex numbers, given in all the 21600 nodes of the core. The information that can be extracted from the complex noise is

the magnitude and the phase of the noise. The magnitude of the neutron noise carries the information of how much the actual neutron flux will deviate from its static value. The phase of the noise can be interpreted as a time shift between the source and its effect at any point in the reactor. A further discussion on the phase of the noise is provided in Chapter 4. The phase of the noise is calculated using the “angle” function in Matlab and it is given in radians.

Fig. 2.2 and 2.3 are an example of the results that can be obtained from the CORE SIM calculation for an absorber of variable strength. In Fig. 2.2 the magnitude of both the fast and thermal noise in the axial channel where the source is located at (i.e. channel (16, 16, K), with K being the axial level), and the noise over the plane of the source (i.e. plane (I, J, 7), with I and J being the index on the x- and y- direction respectively) are plotted. In Fig. 2.3 the phase for both the fast and thermal noise are shown.

In Fig. 2.2 a sharp decrease of both the magnitude of the fast and thermal noise is observed. On the other hand, Fig. 2.3 shows that the phase of the fast and thermal noises has a little deviation throughout the core, and an out of phase behavior of the noise occurs.

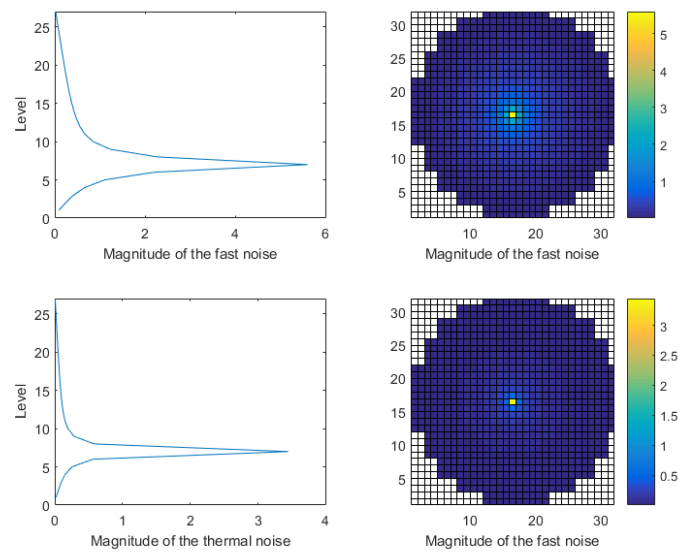


Figure 2.2 The magnitude of the fast noise (top) and the magnitude of the thermal noise (bottom). The plot for the channel is shown on the left while the plot for the level is on the right.

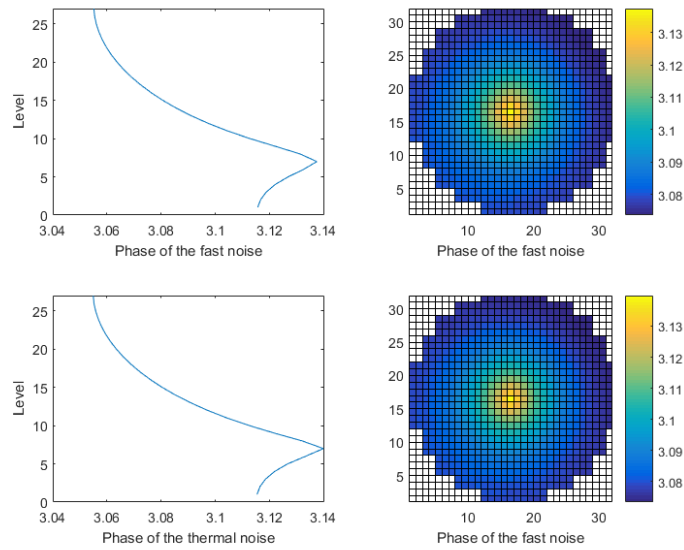


Figure 2.3 The phase of the fast noise (top) and the phase of the thermal noise (bottom). The plot for the channel is shown on the left while the plot for the level is on the right.

## 2.2 Procedure for uncertainty and sensitivity analysis

In order to analyze how the results calculated with CORE SIM can be influenced by the uncertainties in the input parameters, a statistical methodology for the propagation of input uncertainties to the code outputs is applied [10]. The procedure is illustrated in Fig. 2.4.

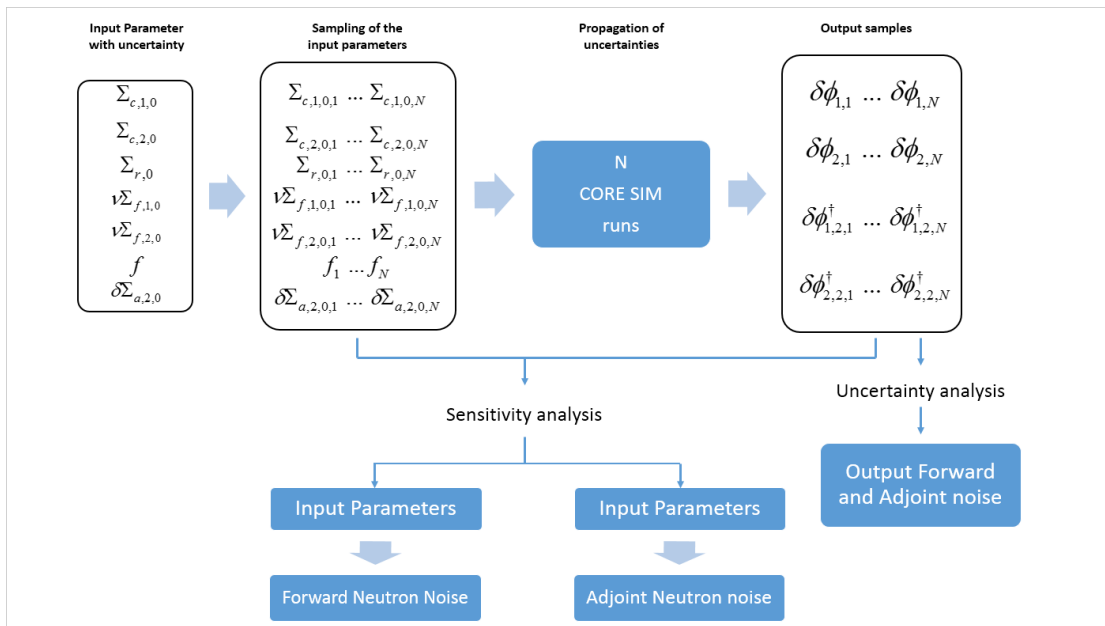


Figure 2.4 Schematic description of the analysis of the propagation of input uncertainties.

In Fig. 2.4, the three subscripts for the adjoint noise respectively indicate the

energy group in which the adjoint noise source is defined, the energy group (as mentioned above, only the thermal adjoint noise is of interest), and the number of the sample.

The macroscopic cross-sections are the main input parameters for CORE SIM, and they are a typical source of uncertainty. The noise source is a local perturbation of the thermal absorption cross-section. Because of the randomness or the lack of knowledge of the noise source, uncertainties are also introduced into the strength and the frequency of the noise source. In addition, it is interesting to see how the neutron noise calculation can be affected by possible deviations from the nominal noise source. The possible uncertainties of the diffusion coefficients for either the fast or thermal group are not included in the study.

Once the input parameters with uncertainties are chosen, the next step is to statistically describe the uncertainties with probability distribution functions (pdfs). A rigorous approach would require the estimation of the pdfs from experimental data. In the current work, the pdfs for the input uncertainties are assumed and two types are selected: the uniform distribution and the normal distribution.

With the uncertain input parameters and their associated “pdfs” settled, a sample of size  $N$  can be generated for each uncertain input parameter, hence  $N$  sets of input parameter are generated. For each of these sets, a neutron noise calculation is performed using CORE SIM. Consequently, samples of size  $N$  for the output variables are obtained (see Fig. 2.4).

In nuclear safety analysis, output uncertainties are usually quantified in terms of tolerance limits. According to the requirements on the tolerance limits, the number of calculations  $N$  can be determined. The minimum number of runs for a two-sided tolerance limit that includes at least a fraction  $\beta$  of the possible results with a probability of  $\alpha$  or greater, is given by the Wilk’s formula [11]:

$$1 - \alpha^N - N(1 - \alpha)\alpha^{N-1} \geq \beta. \quad (2.48)$$

The minimum number of runs for different cases of  $\alpha$  and  $\beta$  are summarized in Table 2.4.

Table 2.4 Minimum number of calculations needed for typical values of  $\alpha$  and  $\beta$

$\alpha \backslash \beta$	0.9	0.95	0.99
0.9	38	77	388
0.95	46	93	473
0.99	64	130	662

The nuclear regulation authorities usually request  $\alpha$  and  $\beta$  to be equal to 0.95, thus uncertainty analysis can be based on 93 runs. However, since the computation time of each run is reasonably short, 500 calculations were used for this thesis. As

discussed later, such a high number of calculations also improves the confidence level of sensitivity analysis.

## 2.3 Uncertainty in the input parameters

Each of the input parameters needs a probability density function that describes how its value can vary because of its uncertainty. In this work, the values for an uncertain input parameter are assumed to be uniformly or normally distributed, so they are generated from the uniform distribution or from the normal distribution.

For the case of a uniform pdf, the values of one uncertain input parameter is generated in the interval  $[\bar{X} - 0.05 \times \bar{X}, \bar{X} + 0.05 \times \bar{X}]$ , where  $\bar{X}$  is the reference value of the uncertain input parameter.

For the case where the uncertain input parameters are normally distributed, the distributions are taken as:

$$f(x | \mu = \bar{X}, \sigma = 0.025 \times \bar{X}) = \frac{1}{\sqrt{2\pi\sigma^2}} e^{-\frac{(x-\mu)^2}{2\sigma^2}}. \quad (2.49)$$

The standard deviation of the normal distribution is chosen to be 2.5% of the reference values of each input parameter, so that the range of the possible values that the uncertain input parameters can take for the normal cases are similar to the uniform case.

The core is discretized into 21600 nodes, and the macroscopic cross-sections need to be specified for each node. In the current work, an independent random sample is generated for each type of macroscopic cross-section and for each node in the core. Then 21600 independent random samples for each cross-section are created (one for each node). Each independent random sample contains 500 values, one for each of the 500 runs. An example of random samples for the removal cross-section is given in Fig. 2.5. The random samples are generated with a uniform and a normal distribution, for node (16, 16, 7) and for the 500 runs.

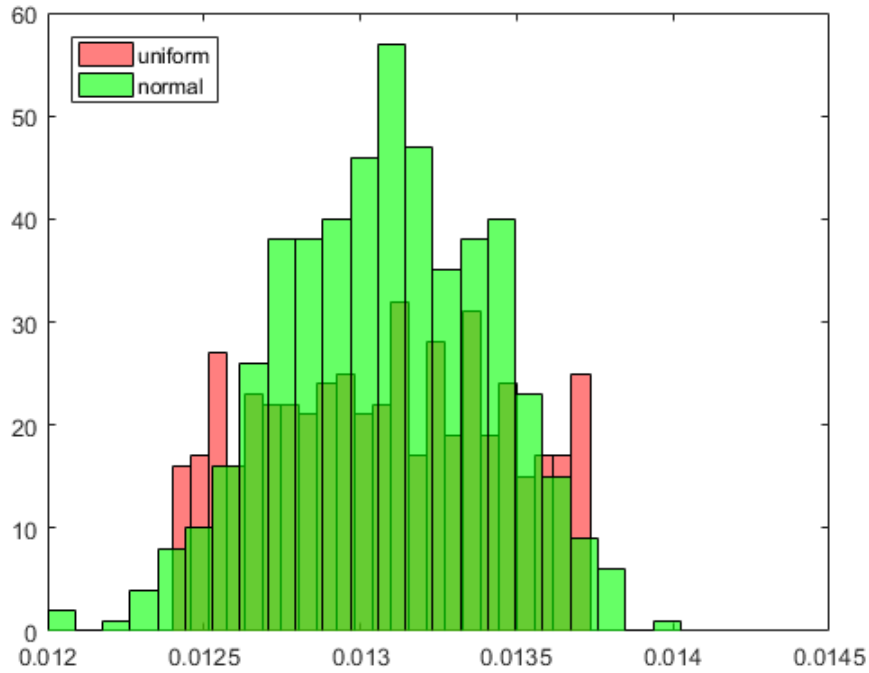


Figure 2.5 The random values generated for the removal cross-section in the node (16, 16, 7) for the 500 runs from a uniform distribution (red) and a normal distribution (green).

Figure 2.5 shows that the range of the possible values for both the uniform and the normal case are similar.

In order to solve the forward and adjoint problems (see Eq. (2.22) and Eq. (2.31)), the input macroscopic cross-sections required are: the macroscopic absorption cross-sections in both groups, the macroscopic fission cross-sections in both groups multiplied by the average number of neutrons produced per fission ( $\nu$ ), the macroscopic removal cross-section.

The macroscopic absorption cross-section is the sum of two contributions:

- The capture of neutrons: the neutrons are captured by the target nucleus and an isotope nucleus of the target is formed.
- The fission reaction: the absorption of the neutron causes the target nucleus to be in an excited state and fission occurs.

The following expression can be then written:

$$\Sigma_a = \Sigma_f + \Sigma_c. \quad (2.50)$$

In view of this, the uncertainties introduced in the fission and in the capture cross-section influence the absorption cross section. Although the absorption cross-section is used as the input for the calculations of CORE SIM, uncertainty is introduced into the capture and fission cross-section independently and the sum of these two parameters is used as the input absorption cross-section.

The procedure is described in the following. The fission cross section is not directly available since we only have the reference value for  $\nu\Sigma_f$ , i.e. the fission cross section is multiplied by the average number of neutrons produced per fission. The value of the average number of neutrons produced per fission for the current calculations is taken to be  $\nu' = 2.44$ , which is the typical value for U-235 based fuel, and, in the current work, it is assumed to be fixed. The reference value of the fission cross-sections are then calculated according to:

$$\Sigma_{f,g,0} = \frac{\nu\Sigma_{f,g,0}}{\nu'} \quad (2.51)$$

where  $g=1$  and  $g=2$  corresponds to the fast and thermal group respectively.

Then the mean value of the capture cross sections are calculated as:

$$\Sigma_{c,g,0} = \Sigma_{a,g,0} - \Sigma_{f,g,0} \quad (2.52)$$

The uncertainties are introduced into  $\nu\Sigma_{f,g,0}$  and  $\Sigma_{r,0}$  using:

$$\Sigma^* = \Sigma_0 + \alpha \cdot \Sigma_0 \quad (2.53)$$

where  $\alpha$  is a random number between -0.05 and 0.05 according to a uniform distribution, or generated from a normal distribution with a mean value of  $\Sigma_0$  and a standard deviation of  $0.025 \times \Sigma_0$ . The "star" superscript indicates the generated random value for the macroscopic cross-section. The value of the random number for  $\nu\Sigma_f$  is saved as  $\alpha_f$ .

The uncertainty of the absorption is obtained by summing up the random values of the capture cross-section and of the fission cross-section. Thus uncertainty is introduced into the capture cross-sections according to:

$$\Sigma_{c,g,0}^* = \Sigma_{c,g,0} + \alpha_c \cdot \Sigma_{c,g,0} \quad (2.54)$$

where the random number  $\alpha_c$  is generated independently from other random numbers used for the other cross sections. The random value for the fission cross-section is generated using:

$$\Sigma_{f,g,0}^* = \Sigma_{f,g,0} + \alpha_f \cdot \Sigma_{f,g,0} \quad (2.55)$$

The random number used in Eq. (2.55) is the same as the one used in the perturbation of  $\nu\Sigma_f$ . Finally the random value for the absorption cross section can be obtained by using the combined random value of fission and capture:

$$\Sigma_{a,g,0}^* = \Sigma_{c,g,0}^* + \Sigma_{f,g,0}^* = \Sigma_{a,g,0} + \alpha_c \cdot \Sigma_{c,g,0} + \alpha_f \cdot \Sigma_{f,g,0} \quad (2.56)$$

At this stage all the cross-sections needed for the input of CORE SIM are ready to be used for the uncertainty and sensitivity analysis.

The above procedure is such that the absorption cross-section is not uniformly distributed because the summation of two uniformly distributed variables leads to variable with a trapezoidal distribution. This is discussed in Chapter 3 with the uncertainty analysis.

The calculations performed for the forward and adjoint problem are summarized in Table 2.5 and 2.6, respectively.

Table 2.5 Summary of the cases of the calculations made for the forward problem

Case	Independently varied cross-sections	Other uncertain parameters	Number of calculations	Distribution used for input parameters	Description
F1	$\Sigma_{c,1,0}$	$\delta\Sigma_{a,2,0}$ and $f$	500	Uniform Distribution	The amount of variation for each type of cross-section and for each node is different
	$\Sigma_{c,2,0}$				
F2	$\Sigma_{r,0}$			Normal Distribution	
	$\nu\Sigma_{f,1,0}$				
	$\nu\Sigma_{f,2,0}$				

As reported in Table 2.5, the forward noise is evaluated at two points. The first one is the point where the source is located at, i.e. (16, 16, 7). The second one is a point away from the source location, i.e. (16, 7, 7).

To set up consistent relations between the forward and adjoint problem (see Eq. (2.44) and (2.45)), the adjoint calculations performed are chosen as listed in Table 2.6. The adjoint problem, as mentioned earlier, uses the same sets of input parameters as the forward problem, including the static macroscopic cross-sections, the frequency and the strength of the source.

Table 2.6 Summary of the cases of the calculations made for the forward problem with uniformly distributed input parameters

Case	Position of source in the core	Group position of the source	Distribution of the input parameters
G1	(16, 16, 7)	Fast	Uniform Distributions
G2		Thermal	
H1	(16, 7, 7)	Fast	
H2		Thermal	
I1	(16, 16, 7)	Fast	Normal Distributions
I2		Thermal	
J1	(16, 7, 7)	Fast	
J2		Thermal	

## 2.4 Uncertainty analysis of the code output

When all the calculations for input uncertainty propagation are performed, the results are then gathered for both the forward problem and the adjoint problem. In the latter case only the thermal adjoint noise is analyzed, as the fast adjoint noise does not correspond to any forward noise of interest.

From the calculations, samples of the output quantities are available. The analysis is focused on the magnitude and the phase of the forward and adjoint noises. The pdfs underlying these samples are evaluated by plotting the relative histograms. This is done using the “histfit” function in Matlab. The number of bins used for the histograms is 23. In addition, the results obtained from the application of a normal distribution fit and of a nonparametric kernel-smoothing distribution fit, are provided.

The parameters used in the uncertainty analysis are:

- The mean value of the values in a set of data, calculated using:

$$\bar{x} = \frac{x_1 + x_2 + \dots + x_N}{N} \quad (2.57)$$

where  $x$  can be the magnitude or the phase of either the forward or adjoint noise with  $N$  the number of calculations is thus 500.

- The standard deviation of the values in a set of data, calculated using:

$$\sigma = \sqrt{\frac{1}{N-1} \sum_{i=1}^N |x_i - \bar{x}|^2} . \quad (2.58)$$

with the mean value given in Eq. (2.57). The standard deviation quantifies the amount of dispersion of a set of data values.

- The kurtosis of the probability distribution of the results, calculated as:

$$k = \frac{\frac{1}{N} \sum_{i=1}^N (x_i - \bar{x})^4}{\left[ \frac{1}{N} \sum_{i=1}^N (x_i - \bar{x})^2 \right]^2} . \quad (2.59)$$

The kurtosis is also a measure of how peaked the distribution of a set of data is. The kurtosis of a normal distribution is equal to 3. Compared to normal distributions, samples with kurtosis values higher than 3 have a stronger peak and a more rapid decay, thus resulting in “heavier” tail than normal. An example of samples with different kurtosis is illustrated in Fig. 2.6. In the plot on the right, the random numbers generated from a normal distribution have a kurtosis of 2.96, which is very close to the theoretical value of 3. In the plot on the left, the random numbers are consistent with a double exponential distribution, and are characterized by a much more distinct peak. The kurtosis for this set of random numbers is 5.9, much larger than the normal case.

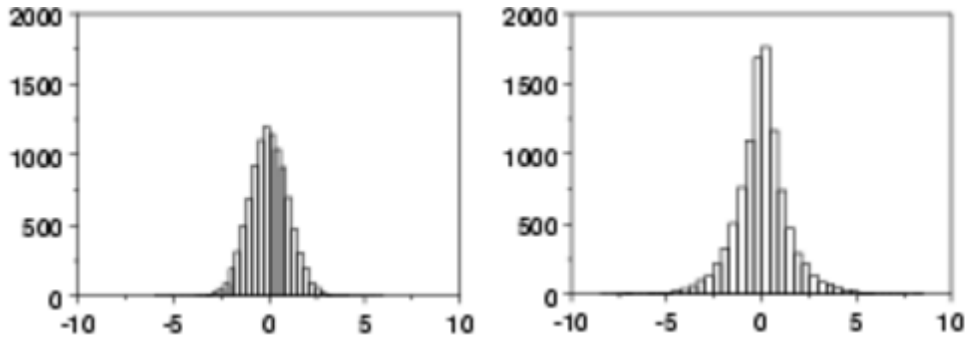


Figure 2.6 10,000 random numbers generated from a normal distribution (left) and from a double exponential (Laplace) distribution (right) [12].

## 2.5 Statistical measures for sensitivity analysis

The input and output samples respectively generated for and obtained from the uncertainty calculations, can be also used for the sensitivity analysis. The aim of sensitivity analysis is to investigate the impact of the input parameters on the calculated outputs. Through sensitivity analysis, the most and less influential input parameters on an output can be identified.

The correlations between the inputs and outputs can be evaluated using different coefficients, such as Pearson correlation coefficient, the Spearman correlation coefficient and so on. The correlation used in this work is the Pearson correlation coefficient [13], [14].

The Pearson correlation coefficient provides a measure of the linear relationship between two variables, given a representative sample of the same size for each of them. In complex computational models, the relationship between the input and output is very unlikely linear and monotonic, however Pearson coefficient are still useful.

In the current work, plots of the Pearson correlation coefficient calculated between pairs of input and output are given. The pair with high Pearson correlation coefficient indeed shows a linear correlation. The coefficient is calculated using the Matlab function “corr”. The Pearson correlation coefficient between an input  $X_j$  and an output  $Y_k$  both represented by a sample of size  $N$ , is calculated according to:

$$c_{jk} = \frac{\sum_{n=1}^N (x_{j,n} - \bar{x}_j)(y_{k,n} - \bar{y}_k)}{\sqrt{\sum_{n=1}^N (x_{j,n} - \bar{x}_j)^2 \sum_{n=1}^N (y_{k,n} - \bar{y}_k)^2}} \quad (2.60)$$

The values of the coefficient ranges from -1 to 1. A value of  $|c_{jk}| = 1$  indicates a perfect linear correlation between the two random variables while a value of  $c_{jk} = 0$  indicates that the two random variables are completely uncorrelated. If the sign of the

coefficient is positive, the two random variables are positively correlated and they change values in the same direction. A negative value means that the two variables vary in opposite directions. Since this is a statistical measure, a certain level of confidence must be specified. A critical value can then be chosen such that if the absolute value of the calculated Pearson correlation coefficient is lower than the critical value, then this pair of random variables are considered to be not statistically significant. The critical value  $z$  is determined by choosing the value for the level of significance  $\alpha$  which gives the probability of rejecting a true hypothesis that two parameters are not correlated. For instance, a significance level of 0.05 indicates a 5% chance that a correlation may be estimated between the pair, even though there is actually no correlation.

The procedure of determining the critical value for a given number of code runs and a chosen significance level is given as follows. If the significance level is chosen to be 0.05 with 500 runs, a value of  $t_1$  is first determined from the two-tailed Student's t-distribution with the degree of freedom  $n = 500 - 2 = 498$ . The value of  $t_1$  obtained is 1.96474. The critical value can be determined as:

$$z_1 = \frac{t}{\sqrt{n + t^2}} \quad (2.61)$$

In the current example  $z_1$  is then equal to 0.08770. This means that, if the absolute value of the Pearson correlation coefficient is greater than  $z_1 = 0.08770$ , the pair of random variables can be considered to be correlated, but there is 5% probability that the correlation is not true.

Instead of the significance level, it is possible to select the critical value to be equal to a prescribed value. In this work, the critical value  $z$  is equal to 0.2. Given 500 values from the calculations, the significance level can be determined as follows. First, the value of  $t$  is obtained according to [15]:

$$t = \frac{z}{\sqrt{1 - z^2}} \sqrt{n} \quad (2.62)$$

For the values of  $z$  and  $n$  given above, the value of  $t$  is equal to 4.55522. Using the two-tailed Student's t-distribution with a degree of freedom of 498, the level of significance is estimated to be  $\alpha = 6.58882 \times 10^{-6}$ . Accordingly if a pair has a value of the Pearson correlation coefficient that is larger than 0.2, and is considered to be correlated, there is only  $6.58882 \times 10^{-4}\%$  probability that this conclusion is wrong, i.e. the correlation is almost certain.

# 3 Uncertainty analysis

Calculations for input uncertainty propagation are performed using CORE SIM. These results allow to investigate the distributions of the output parameters with respect to both uniformly and normally distributed input uncertainties.

A discussion on the uncertainty of the absorption cross-section resulting from the combination of the uncertainties related to the capture and fission cross-section is first given (section 3.1). Then the analysis of the uncertainty distributions of the outputs for the forward calculations (section 3.2) and for the adjoint problem (section 3.3) are presented.

## 3.1 Uncertainty of the absorption cross-sections

As discussed in section 2.3, the uncertainties of the capture and fission cross-sections are sampled independently. The sum of these uncertain cross-sections leads to the uncertain absorption cross-section.

Although the uncertainties for the capture and fission cross-sections are assumed to be uniformly or normally distributed, the uncertainty of the absorption cross-section is not.

In case that a uniform distribution is used for the capture and fission cross-sections, then the pdf associated to the absorption cross-section is a trapezoidal one as proved below.

For the fast group, the probability density function of the fission and capture cross section are:

$$f_{FIS}(x) = \begin{cases} \frac{1}{\Sigma_{f,max} - \Sigma_{f,min}} & \Sigma_{f,min} \leq x \leq \Sigma_{f,max} \\ 0 & \text{otherwise} \end{cases} \quad (3.1)$$

and

$$f_{CAP}(y) = \begin{cases} \frac{1}{\Sigma_{c,max} - \Sigma_{c,min}} & \Sigma_{c,min} \leq y \leq \Sigma_{c,max} \\ 0 & \text{otherwise} \end{cases} \quad (3.2)$$

It is also noticed that the intervals of  $x$  and  $y$  does not overlap each other and thus the calculation can be carried as follows.

The density function of a random variable  $z$  (in this case the absorption cross-section) that is the sum of two uniformly distributed random variables  $x$  and  $y$  (i.e., the fission and the capture cross-section), is given by:

$$f_{ABS}(z) = \int_{-\infty}^{+\infty} f_{FIS}(z-y)f_{CAP}(y)dy. \quad (3.3)$$

Since  $f_{CAP}(y)$  is zero unless  $\Sigma_{c,\min} \leq y \leq \Sigma_{c,\max}$ , the integral becomes:

$$f_{ABS}(z) = \frac{1}{\Sigma_{c,\max} - \Sigma_{c,\min}} \int_{\Sigma_{c,\min}}^{\Sigma_{c,\max}} f_{FIS}(z-y)dy. \quad (3.4)$$

The integrand is 0 unless  $\Sigma_{f,\min} \leq z-y \leq \Sigma_{f,\max}$  or,  $z - \Sigma_{f,\max} \leq y \leq z - \Sigma_{f,\min}$ .

Considering the definition of absorption cross-section, it is not possible that  $z = \Sigma_a < \Sigma_{f,\min} + \Sigma_{c,\min}$  or  $z = \Sigma_a > \Sigma_{f,\max} + \Sigma_{c,\max}$ . Then the pdf is zero for these cases.

In the fast group, the mean (and thus the minimum and maximum value) of the capture cross section is larger than the fission cross section. Hence, different cases can be considered as below.

If  $\Sigma_{f,\min} + \Sigma_{c,\min} \leq z = \Sigma_a < \Sigma_{c,\min} + \Sigma_{f,\max}$ , one has:

$$\begin{aligned} f_{ABS}(z) &= \frac{1}{\Sigma_{c,\max} - \Sigma_{c,\min}} \int_{\Sigma_{c,\min}}^{z - \Sigma_{f,\min}} \frac{1}{\Sigma_{f,\max} - \Sigma_{f,\min}} dy \\ &= \frac{1}{\Sigma_{c,\max} - \Sigma_{c,\min}} \cdot \frac{1}{\Sigma_{f,\max} - \Sigma_{f,\min}} \cdot (z - \Sigma_{f,\min} - \Sigma_{c,\min}) \end{aligned} \quad (3.5)$$

If  $\Sigma_{c,\min} + \Sigma_{f,\max} \leq z = \Sigma_a \leq \Sigma_{f,\min} + \Sigma_{c,\max}$ , one has:

$$\begin{aligned} f_{ABS}(z) &= \frac{1}{\Sigma_{c,\max} - \Sigma_{c,\min}} \int_{z - \Sigma_{f,\max}}^{z - \Sigma_{f,\min}} \frac{1}{\Sigma_{f,\max} - \Sigma_{f,\min}} dy \\ &= \frac{1}{\Sigma_{c,\max} - \Sigma_{c,\min}} \end{aligned} \quad (3.6)$$

If  $\Sigma_{f,\min} + \Sigma_{c,\max} \leq z = \Sigma_a \leq \Sigma_{c,\max} + \Sigma_{f,\max}$ , one has

$$\begin{aligned} f_{ABS}(z) &= \frac{1}{\Sigma_{c,\max} - \Sigma_{c,\min}} \int_{z - \Sigma_{f,\max}}^{\Sigma_{c,\max}} \frac{1}{\Sigma_{f,\max} - \Sigma_{f,\min}} dy \\ &= \frac{1}{\Sigma_{c,\max} - \Sigma_{c,\min}} \cdot \frac{1}{\Sigma_{f,\max} - \Sigma_{f,\min}} \cdot (-z + \Sigma_{f,\max} + \Sigma_{c,\max}) \end{aligned} \quad (3.7)$$

Thus the probability density function for the fast absorption cross-section can be summarized as:

$$f_{ABS_1}(z) = \begin{cases} \frac{(z - \sum_{f,1,\min} - \sum_{c,1,\min})}{(\sum_{c,1,\max} - \sum_{c,1,\min}) \cdot (\sum_{f,1,\max} - \sum_{f,1,\min})}, & \text{if } \sum_{f,1,\min} + \sum_{c,1,\min} \leq z < \sum_{c,1,\min} + \sum_{f,1,\max} \\ \frac{1}{\sum_{c,1,\max} - \sum_{c,1,\min}}, & \text{if } \sum_{c,1,\min} + \sum_{f,1,\max} \leq z \leq \sum_{f,1,\min} + \sum_{c,1,\max} \\ \frac{(-z + \sum_{f,1,\max} + \sum_{c,1,\max})}{(\sum_{c,1,\max} - \sum_{c,1,\min}) \cdot (\sum_{f,1,\max} - \sum_{f,1,\min})}, & \text{if } \sum_{f,1,\min} + \sum_{c,1,\max} < z \leq \sum_{c,1,\max} + \sum_{f,1,\max} \\ 0, & \text{otherwise} \end{cases} \quad (3.8)$$

For the thermal group, a similar result can be obtained. The difference in the thermal group is that the interval where the values of the thermal fission cross section lies is larger than the interval where the thermal capture lies, i.e. the opposite to the situation of the fast cross sections. The density function for the thermal absorption cross section is given by:

$$f_{ABS_2}(z) = \begin{cases} \frac{(z - \sum_{f,2,\min} - \sum_{c,2,\min})}{(\sum_{c,2,\max} - \sum_{c,2,\min}) \cdot (\sum_{f,2,\max} - \sum_{f,2,\min})}, & \text{if } \sum_{f,2,\min} + \sum_{c,2,\min} \leq z < \sum_{c,2,\max} + \sum_{f,2,\min} \\ \frac{1}{\sum_{f,2,\max} - \sum_{f,2,\min}}, & \text{if } \sum_{c,2,\max} + \sum_{f,2,\min} \leq z \leq \sum_{f,2,\max} + \sum_{c,2,\min} \\ \frac{(-z + \sum_{f,2,\max} + \sum_{c,2,\max})}{(\sum_{c,2,\max} - \sum_{c,2,\min}) \cdot (\sum_{f,2,\max} - \sum_{f,2,\min})}, & \text{if } \sum_{f,2,\max} + \sum_{c,2,\min} < z \leq \sum_{c,2,\max} + \sum_{f,2,\max} \\ 0, & \text{otherwise} \end{cases} \quad (3.9)$$

The theoretical density functions given in Eq. (3.8) and (3.9) are compared with the histograms estimated from the samples obtained with the 500 calculations. In the specific example the absorption cross-section is the one associated to the point (16, 7, 7).

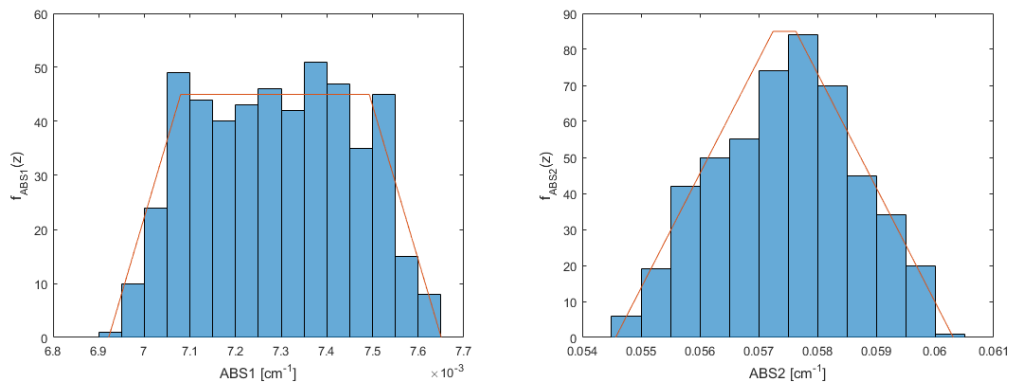


Figure 3.1 The theoretical curve and the actual sampled fast (left) and thermal (right) absorption cross section at the node (16, 7, 7) for the 500 runs made.

The curves are scaled to the height of the histogram for the purpose of comparison, since the actual pdfs given in Eq. (3.8) and (3.9) are larger. As can be seen in the figure, the distribution of the input absorption cross section is no longer a uniform distribution but more values are found to be close to the mean value.

In the calculations based on normally distributed input uncertainties, the uncertain absorption cross-sections also follow a normal distribution. In fact when two independent random variables are normally distributed, i.e.:

$$\begin{aligned} X &\sim N(\bar{X}, \sigma_X^2) \\ Y &\sim N(\bar{Y}, \sigma_Y^2) \end{aligned} \tag{3.10}$$

then the sum of them provides a random variable  $Z = X + Y$  that is still normally distributed. The resulting pdf for Z is such that:  $Z \sim N(\bar{X} + \bar{Y}, \sigma_X^2 + \sigma_Y^2)$ .

## 3.2 Output uncertainties in the forward problem

### 3.2.1 Results from input samples with uniform distributions

The output distributions are given in terms of histograms and distribution fits. In Fig. 3.2 and 3.3 the results for the magnitude and the phase of the calculated noise for two points in Case F1 (Forward problem with uniformly distributed uncertain input parameters) are shown. Figure 3.2 is for the position where the noise source is, i.e. point (16, 16, 7). Figure 3.3 is for the position away from the noise source which is the point (16, 7, 7).

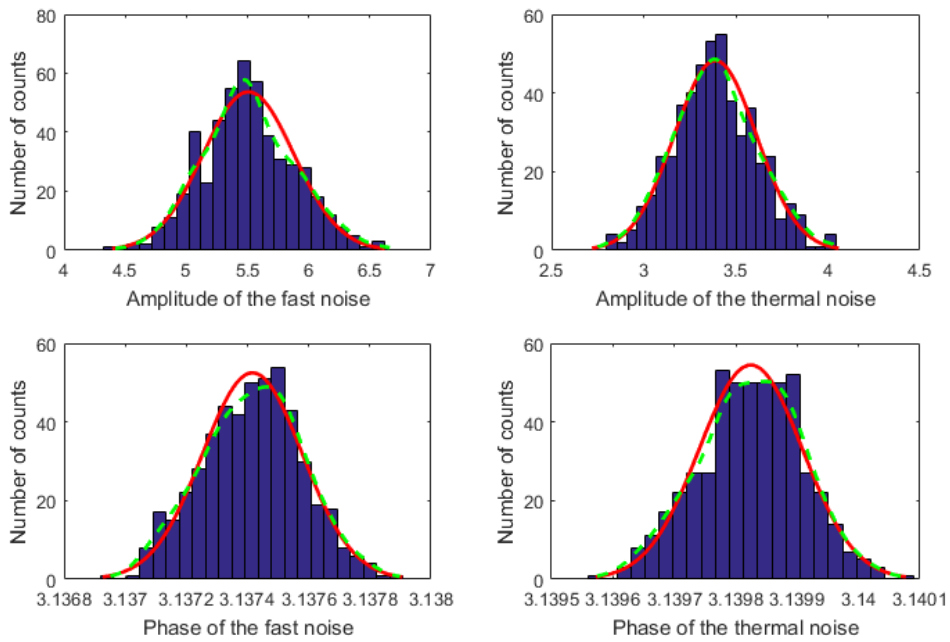


Figure 3.2 Distributions of the amplitude (top) and phase (bottom) of the noise at point (16,16,7), for case F1. Normal density function estimator (red solid line); non-parametric kernel-smoothing distribution fit (green dashed line).

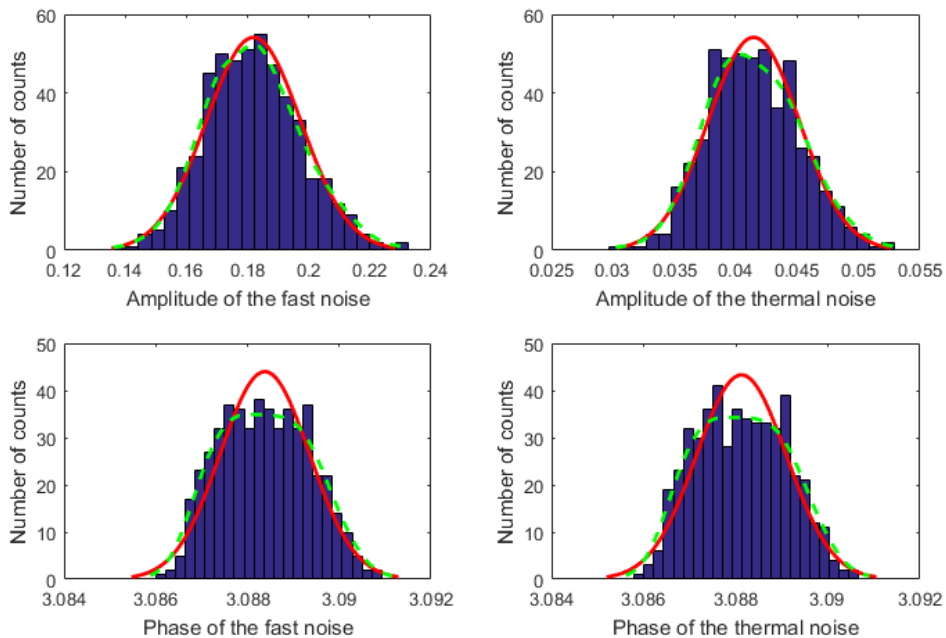


Figure 3.3 Distributions of the amplitude (top) and phase (bottom) of the noise at point (16,7,7), for case F1. Normal density function estimator (red solid line); non-parametric kernel-smoothing distribution fit (green dashed line).

The mean, standard deviation and kurtosis values for the plots above will be given in Table 3.1 together with the normal case F2.

### 3.2.2 Results from input samples with normal distributions

The sensitivity analysis presented in the next chapter is based on input samples with uniform distribution. However, it is of interest to study how the results can be affected by a different choice of probability density function for generating the input samples. Hence, input samples with normal distributions whose standard deviation is equal to 2.5% of the mean values. Such a standard deviation allows to have comparable ranges with the ones from uniform distributions.

Figure 3.4 shows the histogram and the distribution estimations for the magnitude and phase of the noise in the case F2, at point (16, 16, 7). Similarly Fig. 3.5 shows the results at point (16, 7, 7).

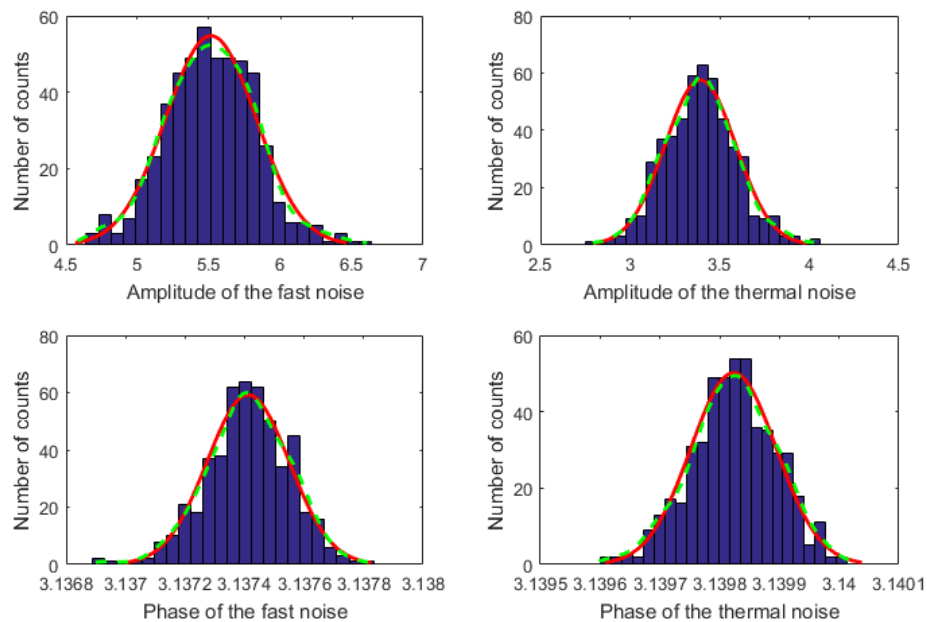


Figure 3.4 Distributions of the amplitude (top) and phase (bottom) of the noise at point (16,16,7), for case F2. Normal density function estimator (red solid line); non-parametric kernel-smoothing distribution fit (green dashed line).

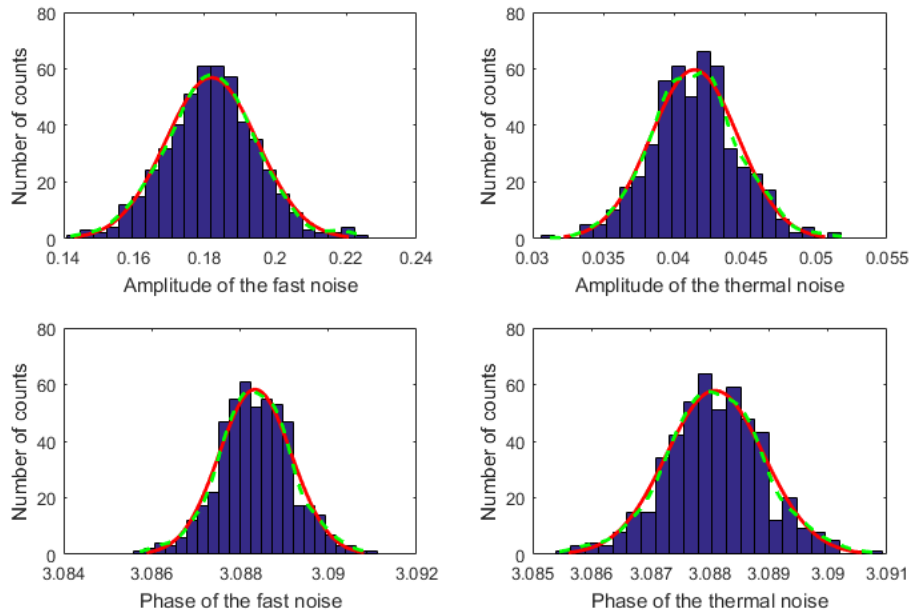


Figure 3.5 Distributions of the amplitude (top) and phase (bottom) of the noise at point (16,7,7), for case F2. Normal density function estimator (red solid line); non-parametric kernel-smoothing distribution fit (green dashed line).

### 3.2.3 Comparison between the uniform and normal cases

The simulations where the input parameters are associated with a normal density function are labelled as the normal case. Similarly, the uniform case is related to the input parameters being sampled uniformly. As discussed in section 3.1, the uncertainty is not directly introduced in the absorption cross section, so this leads to non-uniform and non-normal distributions for the latter.

The distributions of the results are close to a Gaussian for both cases. This outcome suggests that the distribution of the output may be rather insensitive to how the input uncertainties are distributed.

The two cases are compared in Table 3.1 for point (16,16,7) and Table 3.2 for point (16,7,7).

Table 3.1 The mean, standard deviation and kurtosis values for the noise at point (16, 16, 7).

Point (16, 16, 7)	Mean		Standard deviation		Kurtosis	
	Uniform	Normal	Uniform	Normal	Uniform	Normal
$ \delta\phi_1 $	5.50796	5.51375	0.37141	0.31668	2.92743	3.27654
$ \delta\phi_2 $	3.38934	3.39243	0.22327	0.1974	2.88685	3.22559
$\angle\delta\phi_1$	3.13742	3.13741	1.634E-04	1.381E-04	2.69854	3.30114
$\angle\delta\phi_2$	3.1398	3.13982	8.419E-05	7.155E-05	2.82112	2.90292

Table 3.2 The mean, standard deviation and kurtosis values for the noise at point (16, 7, 7).

Point (16, 7, 7)	Mean		Standard deviation		Kurtosis	
	Uniform	Normal	Uniform	Normal	Uniform	Normal
$ \delta\phi_1 $	0.18195	0.18188	0.01547	0.01296	3.01150	3.40933
$ \delta\phi_2 $	0.04146	0.04141	0.00372	0.00307	2.86447	3.29889
$\angle\delta\phi_1$	3.08838	3.0883	9.701E-04	8.212E-04	2.22584	3.33059
$\angle\delta\phi_2$	3.0881	3.08809	9.765E-04	8.270E-04	2.22199	3.33221

It is then observed that:

- For the magnitude of the noise
  - The mean value of the normal cases is similar to the uniform cases.
  - The standard deviation of the normal case is smaller than the uniform case. The random input values generated from the normal distribution has a standard deviation of 2.5% of their mean values. As can be seen in the example given in Fig. 2.5 the range of possible values that the cross-section can take, is larger in the normal case. In the normal case, the probability that the value is beyond the range of the uniform case is only about 5%. Thus with the values of the input parameters more centered to their mean value in the normal cases than in the uniform cases, a smaller standard deviation for the results of the normal cases are observed.
  - As explained in Chapter 2, the value of the kurtosis describes how peaked is a distribution or how concentrated are the values in a sample are to the mean value. The kurtosis values in the uniform case are smaller than 3

(except for the amplitude of the fast noise at point (16,7,7)) and they are always smaller than the values for the normal case. In the latter the values are greater than 3. This may indicate that the use of uniform distributions leads to somewhat of flatter distributions of the output. Nevertheless, all the kurtosis values are close to 3, indicating that the distributions of the magnitude are similar to normal distributions.

- For the phase of the noise
  - The mean value of the phases in the uniform case and the normal case are similar as the phase across the core deviates little from  $\pi$  in the scenario of an absorber of variable strength.
  - When comparing between the uniform and normal cases, the behavior of the standard deviation for the phase is similar to the one for the magnitude. A higher value is obtained in the uniform cases than the normal cases.
  - The kurtosis values for the phases again are close to 3. However, in the uniform case, a low value of the kurtosis is found at the position (16, 7, 7). The histogram of the phases of the noise at position (16, 7, 7) are flatter than the histogram of the phases at the position (16, 16, 7). The kernel smoothing curve also deviates quite significantly from the normal fitting density function. The reason for this behavior can be seen from the sensitivity analysis of the phases. At the point where the noise source is, the input parameters that impact the phases of the noise are the thermal capture, thermal fission, removal cross sections together with the frequency at which the calculation is made. However, at point (16, 7, 7) the only influential parameter on the phase of the noise is the frequency. Since the frequency for the uniform case is also associated to an uncertainty with a uniform density function, this tends to flatten the result of the phase in a significant way.

### 3.3 Output uncertainties in the adjoint problem

As derived in Chapter 2, the thermal adjoint noise induced with a source defined in the fast group, has a corresponding relationship to the fast forward noise (see Eq. (2.44)), while the thermal adjoint noise from a source defined in the thermal group, corresponds to the thermal forward noise (see Eq. (2.45)). The relationships between the magnitude of the forward and adjoint noise can be obtained from Eq. (2.44) and (2.45), and they read:

$$\phi_{2,0}(\mathbf{r}_s) |\delta\phi_{1,2}^\dagger(\mathbf{r}_s, \mathbf{r}_0, \omega)| = |\delta\phi_1(\mathbf{r}_0, \mathbf{r}_s, \omega)| \quad (3.11)$$

and

$$\phi_{2,0}(\mathbf{r}_s) |\delta\phi_{2,2}^\dagger(\mathbf{r}_s, \mathbf{r}_0, \omega)| = |\delta\phi_2(\mathbf{r}_0, \mathbf{r}_s, \omega)|. \quad (3.12)$$

The relationships between the phases are given as:

$$\arg[\delta\phi_{1,2}^\dagger(\mathbf{r}_s, \mathbf{r}_0, \omega)] + \pi = \arg[\delta\phi_1(\mathbf{r}_0, \mathbf{r}_s, \omega)] \quad (3.13)$$

and

$$\arg[\delta\phi_{2,2}^\dagger(\mathbf{r}_s, \mathbf{r}_0, \omega)] + \pi = \arg[\delta\phi_2(\mathbf{r}_0, \mathbf{r}_s, \omega)]. \quad (3.14)$$

From these relationships, the data of the thermal adjoint noise with the adjoint source defined in the fast group can be compared with the magnitude and phase of the fast forward noise. On the other hand, the data of the thermal adjoint noise with the adjoint source defined in the thermal group can be compared to the thermal forward noise.

### 3.3.1 Results from input samples with uniform distributions

The input samples of the cross sections used in the adjoint calculations are the same as the ones used in the forward calculations. Then each run provides results that satisfy Eqs. (3.11)-(3.14).

Figure 3.6 gives the results from the adjoint calculations corresponding to the forward problem F1 (see Table 2.5) where the noise is analyzed at (16, 16, 7). The plots on the left are about the thermal adjoint noise with an adjoint source defined in the fast group, which corresponds to the fast forward noise. The plots on the right show the thermal adjoint noise with an adjoint source defined in the thermal group, which corresponds to the thermal forward noise. Hence the data of the plots on the left are taken from the thermal adjoint noise of case G1 (see Table 2.6) at the position (16, 16, 7), and the plots on the right are taken from the thermal adjoint noise of case G2 (again, see Table 2.6) at the position (16, 16, 7).

In Fig. 3.7 the results from the adjoint calculations corresponding to the forward problem F1 where the noise is analyzed at (16, 7, 7). The data of the left plots are taken from the thermal adjoint noise in case H1 at the position (16, 16, 7), and the plots on the right are taken from the thermal adjoint noise in case H2 at the position (16, 16, 7).

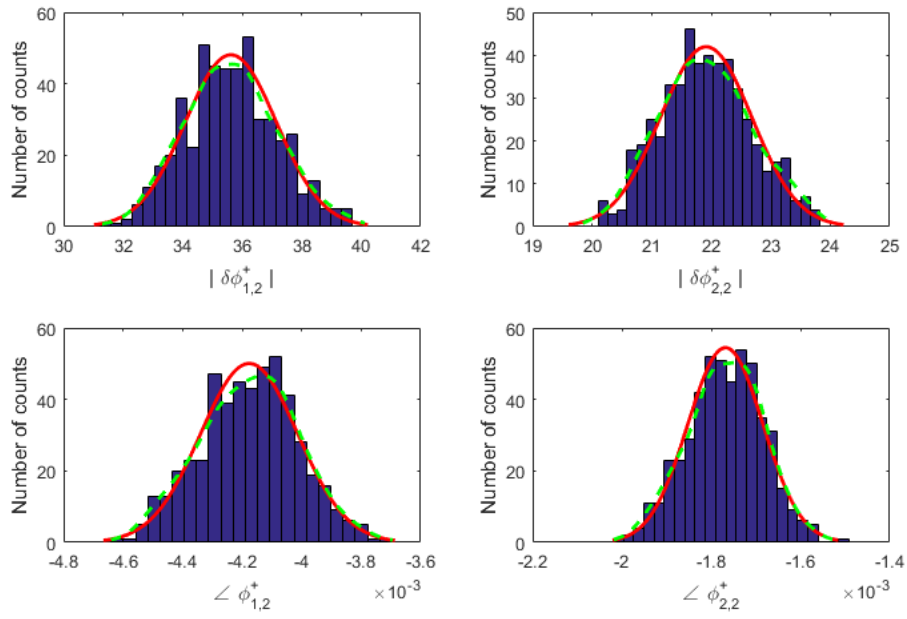


Figure 3.6 The adjoint calculations corresponding to the forward noise evaluated at (16, 16, 7) for the Case F1.

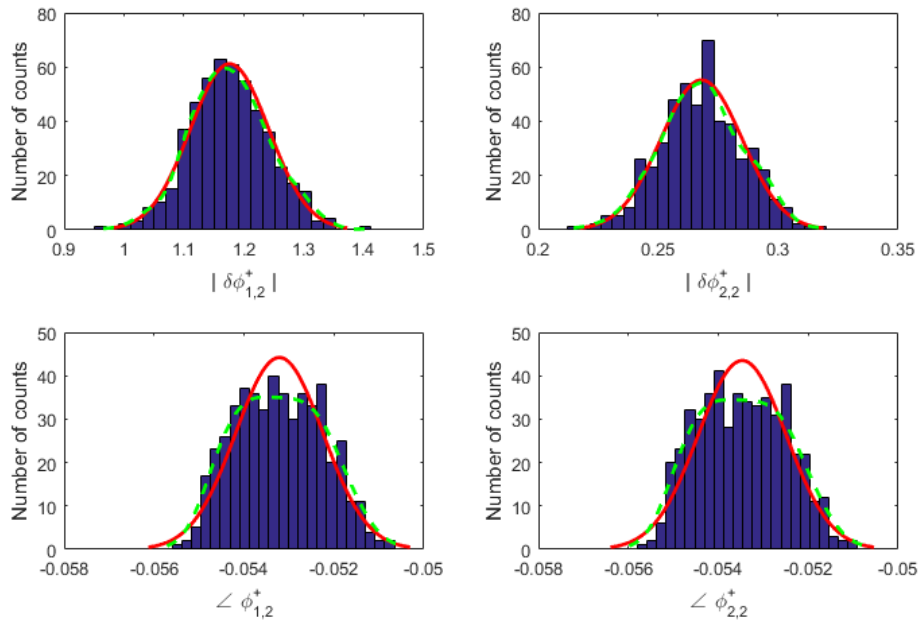


Figure 3.7 The adjoint calculations corresponding to the forward noise evaluated at (16, 7, 7) for the Case F1.

### 3.3.2 Results from input samples with normal distributions

In Fig. 3.8 the results from the adjoint calculations correspond to the forward problem F2 (see Table 2.5) where the noise is analyzed at (16, 16, 7). The data of the plots on the left are taken from the thermal adjoint noise in case I1 (see Table 2.6) at the position (16, 16, 7), and the plots on the right are taken from the thermal adjoint noise in case I2 (see Table 2.6) at the position (16, 16, 7).

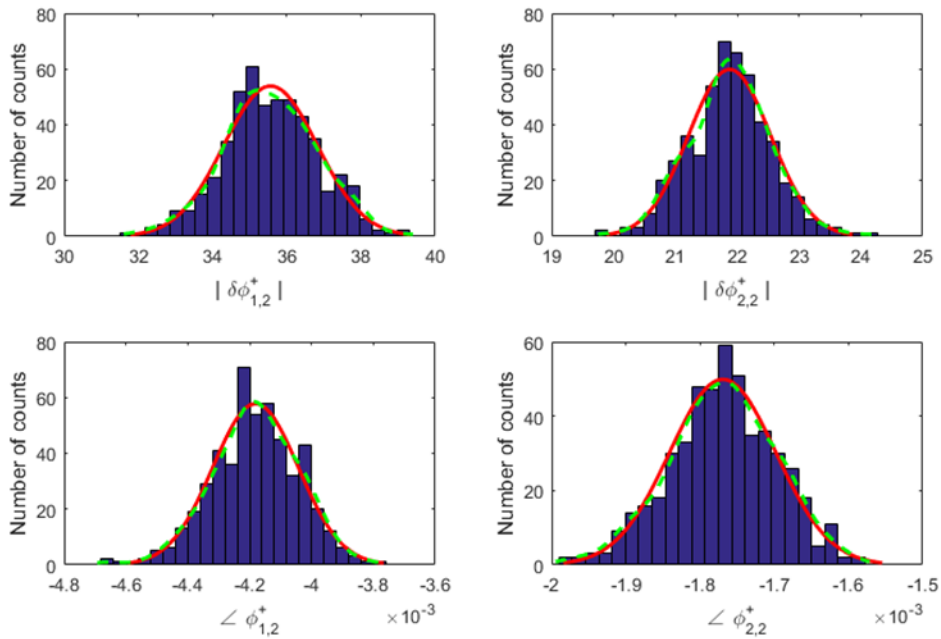


Figure 3.8 The adjoint calculations corresponding to the forward noise evaluated at (16, 16, 7) for the Case F2, both with normally distributed input parameters.

In Fig. 3.9 the results from the adjoint calculations correspond to the forward problem F2 where the noise is analyzed at (16, 7, 7). The data of the plots on the left are taken from the thermal adjoint noise of case J1 at the position (16, 16, 7), and the plots on the right are taken from the thermal adjoint noise of case J2 at the position (16, 16, 7).

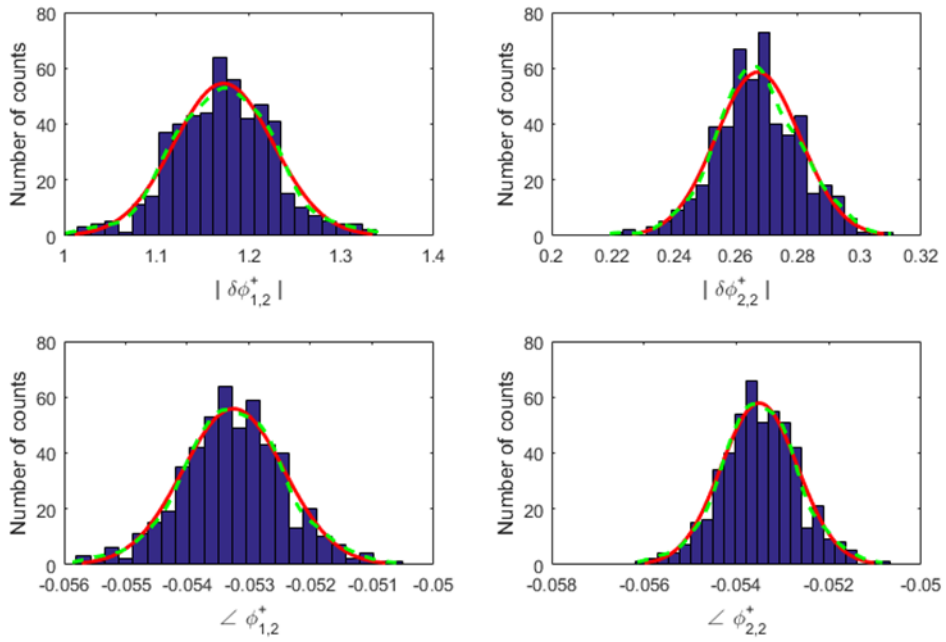


Figure 3.9 The adjoint calculations corresponding to the forward noise evaluated at (16, 7, 7) for the Case F2, both with normally distributed input parameters.

### 3.3.3 Comparison between the uniform and normal cases

The mean, standard deviation and kurtosis of the histograms given in Figs. 3.6-3.9, are summarized in Table 3.3 for the adjoint calculations that correspond to the forward noise evaluated at point (16, 16, 7); and in Table 3.4 for the adjoint calculations that correspond to the forward noise at point (16, 7, 7).

Table 3.3 The mean, standard deviation and kurtosis values for the adjoint noise corresponding to the forward noise at point (16, 16, 7).

Corresponding Forward Point (16, 16, 7)	Mean		Standard deviation		Kurtosis	
	Uniform	Normal	Uniform	Normal	Uniform	Normal
$ \delta\phi_{1,2}^\dagger $	35.6215	35.5647	1.53408	1.25771	2.74896	2.99257
$ \delta\phi_{2,2}^\dagger $	21.9152	21.8773	0.76998	0.66309	2.57065	3.39446
$\angle\delta\phi_{1,2}^\dagger$	-0.00418	-0.00418	1.634E-04	1.381E-04	2.69854	3.30114
$\angle\delta\phi_{2,2}^\dagger$	-0.00177	-0.00177	8.419E-05	7.155E-05	2.82112	2.90292

Table 3.4 The mean, standard deviation and kurtosis values for the adjoint noise corresponding to the forward noise at point (16, 7, 7).

Corresponding Forward Point (16, 7, 7)	Mean		Standard deviation		Kurtosis	
	Uniform	Normal	Uniform	Normal	Uniform	Normal
$ \delta\phi_{1,2}^\dagger $	1.17590	1.17261	0.06549	0.05373	3.14433	3.31726
$ \delta\phi_{2,2}^\dagger $	0.26797	0.26698	0.01697	0.01361	2.87900	3.34956
$\angle\delta\phi_{1,2}^\dagger$	-0.05321	-0.05325	9.701E-04	8.212E-04	2.22584	3.33059
$\angle\delta\phi_{2,2}^\dagger$	-0.05347	-0.05350	9.765E-04	8.270E-04	2.22199	3.33221

From the comparison of these results, it can be seen that the output distributions of the adjoint calculations are rather insensitive to the input distributions. In both cases for the adjoint calculations, the results are approximately distributed according to a normal, as the comparison between the kernel smoothing curve and the normal fitting curve shows. In particular, the calculated mean values are similar; and smaller standard deviation values and higher kurtosis values are estimated in the normal case.

Such an outcome is consistent with the one for the forward case (see section 3.2.3).

### 3.4 Comparison between the forward and adjoint calculations

The comparison is made only for calculations with uniformly distributed input parameters, as the same conclusions can be drawn for the normal cases.

By comparing Table. 3.1 and 3.3 (or 3.2 and 3.4), it can be observed that:

- For the magnitude of the noise
  - The mean values of the magnitude of the forward noise are smaller than the adjoint noise. According to Eq. (3.11) and (3.12), the magnitude of the forward noise is obtained by multiplying the thermal adjoint noise by the thermal static flux. The thermal static flux calculated in the core is smaller than unity, thus the magnitude of the adjoint noise is larger than the magnitude of the forward noise.
  - As the values of the magnitude of the adjoint noise are larger than the values of the forward noise, the standard deviation is also rescaled and larger for the adjoint noises.

- The lower value of the kurtosis for the adjoint calculations implies that the distributions are less peaked than the ones obtained from the forward calculations. Then the uncertainty in the input parameters has a slightly larger impact on the adjoint calculations.
- For the phase of the noise
  - The mean value is shifted by  $\pi$  according to Eq. (3.13) and (3.14).
  - The standard variation remains the same because the shift of a random variable  $X$  by adding a constant  $c$  has no effect:

$$\sigma(X + c) = \sigma(X) \quad (3.15)$$

However, since the absolute mean value of the phase becomes smaller while the standard deviation remains the same in the adjoint problem, then the ratio  $\sigma/|\mu|$  is considerably larger compared to the forward problem. The interval of the possible value for both cases is the same, but for the adjoint problem, it is associated to a smaller mean value. Thus the range of possible values with respect to the mean value is larger.

- The kurtosis values are close. If the output results for the adjoint problem are denoted as the random variable  $Y$  and the results for the forward problem are denoted as the random variable  $X$ , then their kurtosis values are equal to each other because of the shift of  $\pi$ :

$$k(X) = \frac{E(X - \mu)^4}{\sigma_x^4} = \frac{E[(Y + \pi) - (\mu + \pi)]^4}{\sigma_Y^4} = k(Y) \quad (3.16)$$

The similar kurtosis and standard deviation value lead to distributions that do not differ much from each other.



## 4 Sensitivity analysis

The sensitivity analysis is based on the calculations in which the uncertainty of the input parameters is uniformly distributed.

### 4.1 Sensitivity analysis for the forward problem

The sensitivity analysis for the forward problem is based on the calculations for the case F1 (see Table 2.5).

The forward noise source is placed at the point (16, 16, 7) and the sensitivity analysis is carried out for the noise located at the point where the source is, and at another point away from the source but on the same level as the source, i.e. (16, 7, 7). The positions of the source and of the noise are illustrated in Fig. 4.1.

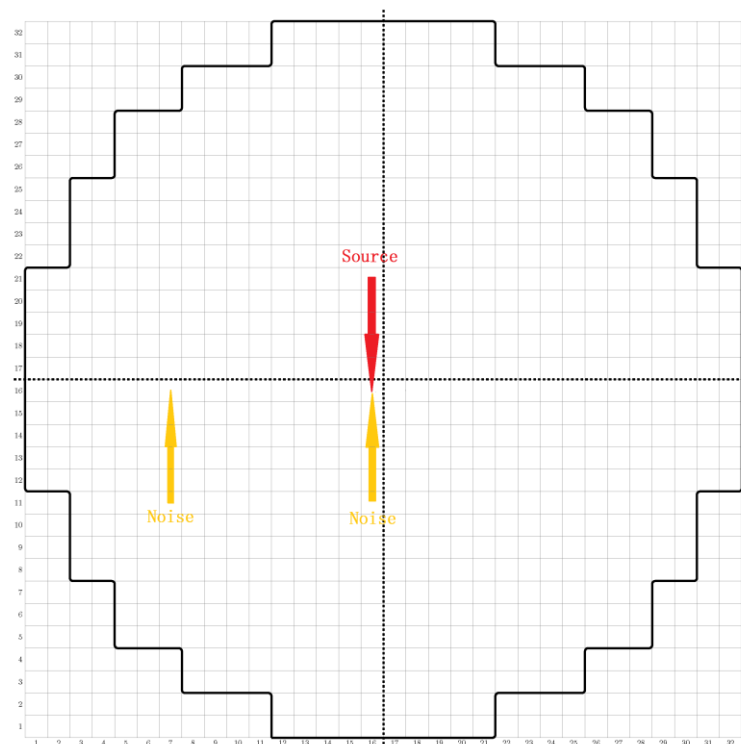


Figure 4.1 Axial level 7 of the core nodalization: position of the source (red) and the positions at which the noise is evaluated (orange).

### 4.1.1 Correlations between uncertain input parameters and noise in the same node

The Pearson correlation coefficients are calculated between the cross-sections in one node and the magnitude and the phase of the noise in the same node. The correlations between the source frequency and the noise, and between the noise source strength and the noise are also included.

In Figs. 4.2 and 4.3 the results are shown for the points (16, 16, 7) and (16, 7, 7), respectively.

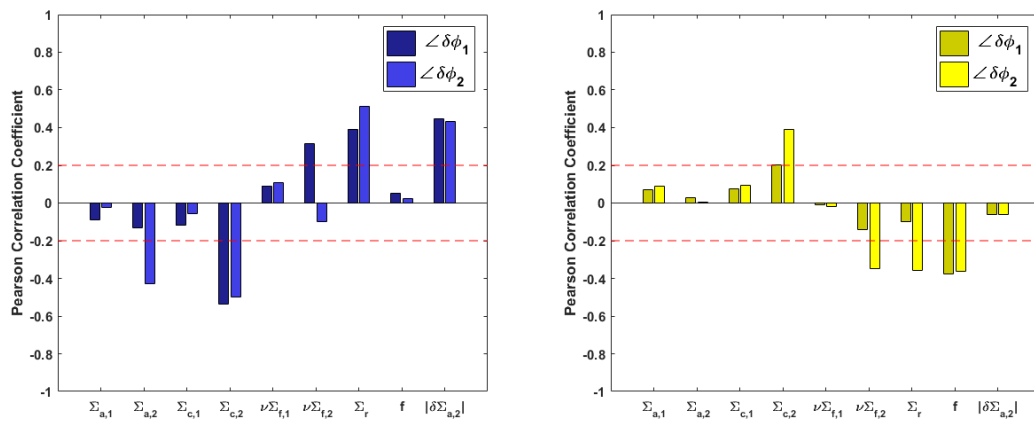


Figure 4.2 The Pearson correlation coefficient between the cross sections at the point (16, 16, 7), the frequency, the source strength and the noise at (16, 16, 7) for the Case F1. The plot for the magnitude is shown on the left and the phase on the right.

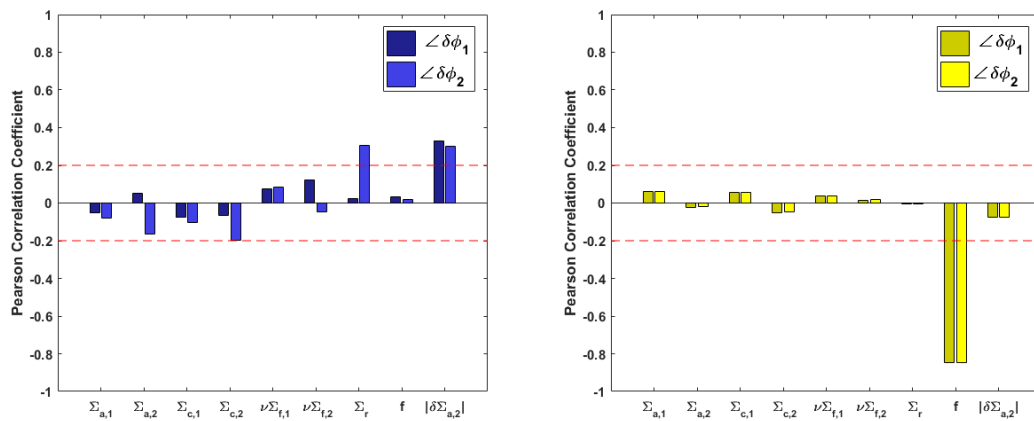


Figure 4.3 The Pearson correlation coefficient between the cross sections at the point (16, 7, 7), the frequency, the source strength and the noise at (16, 7, 7) for the Case F1. The plot for the magnitude is shown on the left and the phase on the right.

### **Magnitude of the noise**

The thermal capture cross-section in the node where the source is, shows a negative correlation to the magnitude of both the fast and thermal noise in the same node. In fact an increase in the thermal capture cross section leads to a decrease in the thermal static flux. Less thermal neutrons induces less fissions, and the fast neutron flux decreases too because less fast neutrons are released from the fissions. As mentioned earlier, the “power reactor noise” is proportional to the square of the static flux, and thus decreasing both the fluxes cause the noise in both groups to decrease as well. The correlation to the magnitude of the fast noise is even slightly stronger than to the thermal noise. The reason might be the capture of one thermal neutron would mean that a fission together with 2-3 fast neutrons are lost. In view of this, the fast flux may be more sensitive to the thermal capture cross-section.

The thermal fission cross-section in the node (16, 16, 7) shows a significant positive correlation to the fast noise and no correlation to the thermal noise in the node (16, 16, 7). This can be explained as follows. When the static fission cross-section increases, more thermal neutrons are absorbed to induce fission. The primary effect would be a decrease in the thermal flux and an increase in the fast flux. This loss of thermal neutrons can be compensated by the more removal (down scattering of fast neutrons). More down-scattered fast neutrons would cause the fast flux to decrease, but such a reduction is largely counterbalanced by the multiple fast neutrons that are produced per fission. Thus, the increase of thermal fission cross-section will result in an increase of the fast flux and consequently the fast forward noise, while the thermal noise is almost unaffected.

The correlation between the thermal absorption cross-section and the noises is a combined effect of the thermal fission cross-section and the thermal capture cross-section. The thermal absorption cross section only shows significant negative correlation to the thermal noise. On the other hand the fast noise is not affected, as the more fissions compensates the more down-scattering and the more thermal captures.

A positive correlation is found between the removal cross-section in the node (16, 16, 7) and the magnitude of both the fast and thermal noise in the node (16, 16, 7). The increase of removal cross-section indicated better moderation of the neutrons and thus more thermal neutrons that have a large probability of inducing fission reactions are produced. This results in both an increase in the thermal flux and fast flux and consequently the fast noise and thermal noise.

The calculations are carried out around the frequency of 1 Hz. As it can be seen in either Fig. 4.2 or Fig. 4.3, the change of frequency does not affect the magnitude of the noise. To explain this behavior, the real part of the dynamic equations can be taken. In fact the imaginary part is very small and the magnitude of the noise can be approximated with the value of the real part. For instance, the complex noise computed at the location of the source is  $-5.5975 + 0.0234i$ , and the magnitude is

5.5975. For the node (16, 7, 7), the complex noise is  $-0.1845 + 0.0098i$ , and the magnitude is 0.1847. So the real part of the noise is very close to the magnitude. The real part of the dynamic equation is derived as follows.

The dynamic equations are:

$$\begin{aligned} \nabla \cdot D_{1,0} \nabla \cdot \delta\phi_1(\mathbf{r}, \omega) - \left[ \Sigma_{a,1,0}(\mathbf{r}) + \frac{i\omega}{v_1} + \Sigma_{r,0}(\mathbf{r}) \right] \cdot \delta\phi_1(\mathbf{r}, \omega) \\ + \frac{\nu \Sigma_{f,1,0}(\mathbf{r})}{k_{eff}} \left( 1 - \frac{i\omega\beta}{i\omega + \lambda} \right) \cdot \delta\phi_1(\mathbf{r}, \omega) + \frac{\nu \Sigma_{f,2,0}(\mathbf{r})}{k_{eff}} \left( 1 - \frac{i\omega\beta}{i\omega + \lambda} \right) \cdot \delta\phi_2(\mathbf{r}, \omega) = 0 \end{aligned} \quad (4.1)$$

$$\begin{aligned} \nabla \cdot D_{2,0} \nabla \cdot \delta\phi_2(\mathbf{r}, \omega) - \left[ \Sigma_{a,2,0}(\mathbf{r}) + \frac{i\omega}{v_2} \right] \cdot \delta\phi_2(\mathbf{r}, \omega) \\ + \Sigma_{r,0}(\mathbf{r}) \cdot \delta\phi_1(\mathbf{r}, \omega) = \phi_{2,0} \delta \Sigma_{a,2}(\mathbf{r}, \omega) \end{aligned} \quad (4.2)$$

The fast noise, thermal noise and the noise source consist of a real and an imaginary part as:

$$X(\mathbf{r}, \omega) = X_{Re}(\mathbf{r}) + iX_{Im}(\mathbf{r}), \quad (4.3)$$

The latter is inserted into Eq. (4.1), and the following expressions are obtained:

$$\begin{aligned} \nabla \cdot D_{1,0} \nabla \left[ \delta\phi_{1,Re}(\mathbf{r}) + i\delta\phi_{1,Im}(\mathbf{r}) \right] \\ - \left[ \Sigma_{a,1,0}(\mathbf{r}) + \frac{i\omega}{v_1} + \Sigma_{r,0}(\mathbf{r}) \right] \cdot \left[ \delta\phi_{1,Re}(\mathbf{r}) + i\delta\phi_{1,Im}(\mathbf{r}) \right] \\ + \frac{\nu \Sigma_{f,1,0}(\mathbf{r})}{k_{eff}} \left( 1 - \frac{i\omega\beta}{i\omega + \lambda} \right) \cdot \left[ \delta\phi_{1,Re}(\mathbf{r}) + i\delta\phi_{1,Im}(\mathbf{r}) \right] \\ + \frac{\nu \Sigma_{f,2,0}(\mathbf{r})}{k_{eff}} \left( 1 - \frac{i\omega\beta}{i\omega + \lambda} \right) \cdot \left[ \delta\phi_{2,Re}(\mathbf{r}) + i\delta\phi_{2,Im}(\mathbf{r}) \right] = 0 \end{aligned} \quad (4.4)$$

$$\begin{aligned} \nabla \cdot D_{2,0} \nabla \left[ \delta\phi_{2,Re}(\mathbf{r}) + i\delta\phi_{2,Im}(\mathbf{r}) \right] - \left[ \Sigma_{a,2,0}(\mathbf{r}) + \frac{i\omega}{v_2} \right] \cdot \left[ \delta\phi_{2,Re}(\mathbf{r}) + i\delta\phi_{2,Im}(\mathbf{r}) \right] \\ + \Sigma_{r,0}(\mathbf{r}) \cdot \left[ \delta\phi_{1,Re}(\mathbf{r}) + i\delta\phi_{1,Im}(\mathbf{r}) \right] = \phi_{2,0}(\mathbf{r}) \left[ \delta \Sigma_{a,2,Re}(\mathbf{r}) + i\delta \Sigma_{a,2,Im}(\mathbf{r}) \right] \end{aligned} \quad (4.5)$$

The real part of the first term in the fast equation is:

$$\nabla \cdot D_{1,0} \nabla \delta\phi_{1,Re}(\mathbf{r}). \quad (4.6)$$

The real part of the second term in the fast equation is:

$$\left[ \Sigma_{a,1,0}(\mathbf{r}) - \frac{\omega}{v_1} + \Sigma_{r,0}(\mathbf{r}) \right] \cdot \delta\phi_{1,Re}(\mathbf{r}). \quad (4.7)$$

Some approximations can be made. Since  $v_1 \gg \omega$ , one can assume that  $\frac{\omega}{v_1} \sim 0$ . In fact,

using the kinetic data given in Table 2.3 with  $\omega = 2\pi f = 6.2832$ , the numerical value

of  $\omega/v_1$  is about  $3.53 \times 10^{-7}$ . The second term becomes:

$$\left[ \Sigma_{a,1,0}(\mathbf{r}) + \Sigma_{r,0}(\mathbf{r}) \right] \cdot \delta\phi_{1,\text{Re}}(\mathbf{r}) \quad (4.8)$$

The real part of the third term in the fast equation is:

$$\frac{v\Sigma_{f,1,0}(\mathbf{r})}{k_{\text{eff}}} \cdot \left[ \left( 1 - \frac{\omega^2\beta}{\omega^2 + \lambda^2} \right) \cdot \delta\phi_{1,\text{Re}}(\mathbf{r}) + \frac{\omega\lambda\beta}{\omega^2 + \lambda^2} \cdot \delta\phi_{1,\text{Im}}(\mathbf{r}) \right] \quad (4.9)$$

For this term, the following approximation is introduced

$$1 - \frac{\omega^2\beta}{\omega^2 + \lambda^2} = 1 - \frac{\beta}{1 + \frac{\lambda^2}{\omega^2}} \xrightarrow{\omega \gg \lambda} 1 - \beta \xrightarrow{\beta \sim 0} 1 \quad (4.10)$$

$$\frac{\omega\lambda\beta}{\omega^2 + \lambda^2} = \frac{\beta}{\frac{\omega}{\lambda} + \frac{\lambda}{\omega}} \xrightarrow{\frac{\lambda}{\omega} \sim 0, \frac{\omega}{\lambda} \gg 0, \beta \sim 0} 0$$

The numerical value of the two expressions in Eq. (4.10), using the kinetic data value given in Table. 2.3 is 0.9944 and  $7 \times 10^{-5}$  respectively. The third term can then be written as:

$$\frac{v\Sigma_{f,1,0}(\mathbf{r})}{k_{\text{eff}}} \cdot \delta\phi_{1,\text{Re}}(\mathbf{r}) \quad (4.11)$$

Similarly the fourth term in the fast equation can be simplified as:

$$\frac{v\Sigma_{f,2,0}(\mathbf{r})}{k_{\text{eff}}} \cdot \delta\phi_{2,\text{Re}}(\mathbf{r}). \quad (4.12)$$

In the real part of the thermal equation the term  $\frac{\omega}{v_2} \delta\phi_{2,\text{Im}}(\mathbf{r})$  can be neglected, since

$v_2 \gg \omega$  and  $\delta\phi_{2,\text{Im}}(\mathbf{r}) \sim 0$ . Under this assumption, the real part of Eq. (4.5) can be written as:

$$\nabla \cdot D_{2,0} \nabla \delta\phi_{2,\text{Re}}(\mathbf{r}) - \Sigma_{a,2,0}(\mathbf{r}) \cdot \delta\phi_{2,\text{Re}}(\mathbf{r}) + \Sigma_{r,0}(\mathbf{r}) \cdot \delta\phi_{1,\text{Re}}(\mathbf{r}) = \phi_{2,0} \cdot \delta\Sigma_{a,2,\text{Re}}(\mathbf{r}) \quad (4.13)$$

In summary, the real part of the noise calculation can be approximated as:

$$\nabla \cdot D_{1,0} \nabla \delta\phi_{1,\text{Re}}(\mathbf{r}) - \left[ \Sigma_{a,1,0}(\mathbf{r}) + \Sigma_{r,0}(\mathbf{r}) \right] \cdot \delta\phi_{1,\text{Re}}(\mathbf{r}) + \frac{v\Sigma_{f,1,0}(\mathbf{r})}{k_{\text{eff}}} \cdot \delta\phi_{1,\text{Re}}(\mathbf{r})$$

$$+ \frac{v\Sigma_{f,2,0}(\mathbf{r})}{k_{\text{eff}}} \cdot \delta\phi_{2,\text{Re}}(\mathbf{r}) = 0 \quad (4.14)$$

$$\nabla \cdot D_{2,0} \nabla \delta\phi_{2,\text{Re}}(\mathbf{r}) - \Sigma_{a,2,0}(\mathbf{r}) \cdot \delta\phi_{2,\text{Re}}(\mathbf{r}) + \Sigma_{r,0}(\mathbf{r}) \cdot \delta\phi_{1,\text{Re}}(\mathbf{r}) = \phi_{2,0} \cdot \delta\Sigma_{a,2,\text{Re}}(\mathbf{r}) \quad (4.15)$$

In the current case of frequencies around 1 Hz, Eq. (4.14) shows that, the real

part which dominates the value of the magnitude of the noise, is not influenced by the frequency.

A change in the strength of the noise source causes the noise to vary with the same trend. This influence decreases with increasing distance from the noise source as expected. Nevertheless, by moving away from the source, the strength of the noise source becomes more and more dominant over the other parameters. In addition, the cross sections at a point away from the source, have almost no impact on the noise calculated. The only contribution from the cross-sections is due to the removal cross section, even though it is weak. This can be seen from Fig. 4.3.

### **Phase of the noise**

When the phase of the fast noise is evaluated at the position where the noise source is, all the input parameters have no significant effect, except the frequency (see Fig. 4.2).

As regards the phase of the thermal noise at the location of the noise source, the relevant correlations are with the thermal capture cross-section, the fission cross-section and the removal cross-section, and with the frequency (again, see Figure 4.2). The thermal capture cross section shows a positive correlation, while the thermal fission and removal cross section shows a negative correlation. The reasons for these correlations are still unclear and further investigations are needed.

The frequency has negative correlations to the phase of both the fast and thermal noise. The correlation with the frequency increases in absolute value as the position for the evaluation of the noise gets away from the source, while the influence of the other parameters vanish (compare Fig. 4.2 and Fig. 4.3).

In Fig. 4.4 the correlation coefficients between the noise and the frequency are given for all the nodes over the plane where the source is placed. The spatial behavior of the correlation is such that the Pearson coefficient reaches values very close to -1 after few nodes from the source, which means that the frequency and the phases are almost negatively linear correlated in a large part of the core. This increase in absolute value of the correlation also indicates that the phase delay of the noise is more sensitive to the change in frequency as the position gets further away from the noise source.

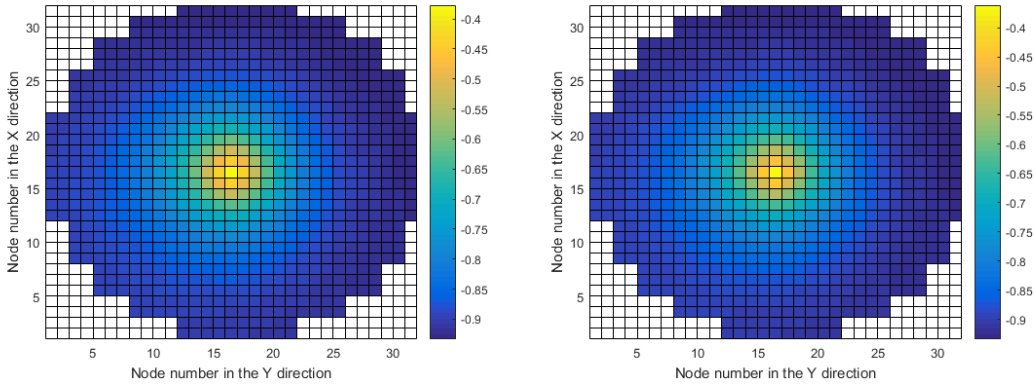


Figure 4.4 The correlation between the frequency and the phase of the fast neutron noise (left) and of the thermal neutron noise (right) at different nodes in level 7.

#### 4.1.2 Pearson correlation coefficient between the thermal capture cross-section over level 7 and the noise in a fixed position

The influence of the cross-sections in other nodes, on the noise calculated at the source point is investigated. For instance, the cross-sections are taken at the point (16, 7, 7), and their correlations with respect to the noise at point (16, 16, 7) are calculated and plotted in Fig. 4.5.

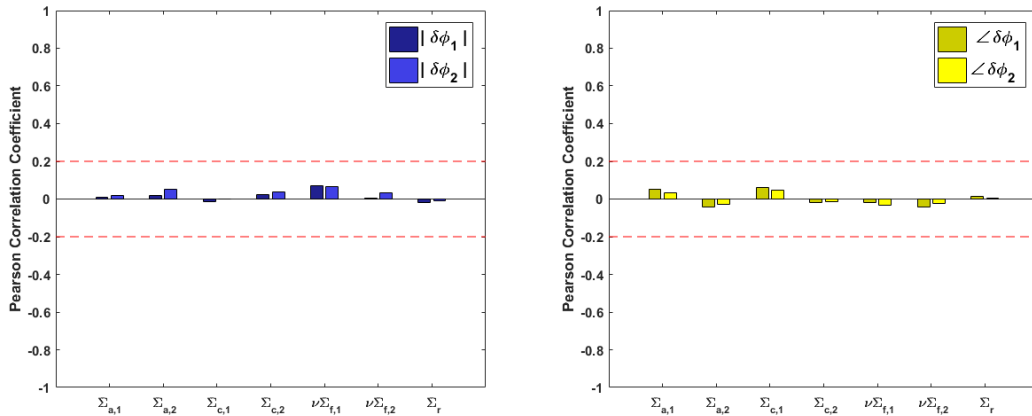


Figure 4.5 Pearson correlation coefficient between each type of cross-section at point (16, 7, 7) and the magnitude of the noise (left), and the phase of the noise (right) at the point where the noise source is.

Figure 4.5 shows that the cross sections in a point away from the source will not influence the noise calculated in the node where the source is. As seen in Fig. 4.2 where the noise is taken at the position of the source, the strongest influence to both the magnitude and the phase of the noise are from the thermal capture cross section of the same node. Thus if there should be any influence from any kind of cross-section in other nodes to the noise calculated in the node (16, 16, 7), it should most probably be thermal capture cross-section. Hence the correlation between this cross-section

taken in all the nodes of axial level 7 and the noise at the position (16, 16, 7) is investigated. The relative Pearson correlation coefficients are calculated and shown in Fig. 4.6.

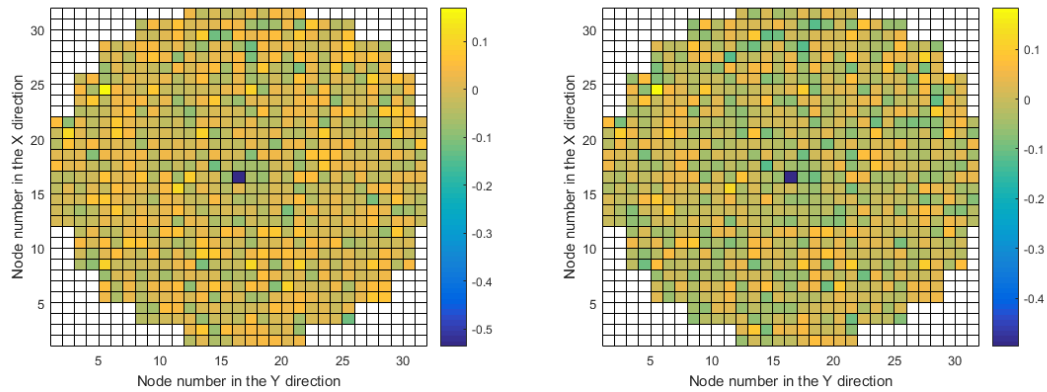


Figure 4.6 The spatial variation of the correlation between the input thermal capture cross sections of the nodes in level 7 and the output the magnitude of the fast (left) and thermal (right) noise at the node (16, 16, 7).

Only the thermal capture cross-section from the same node influences the noise calculated at (16, 16, 7). The value of the Pearson correlation coefficient for the thermal capture cross-section in all the other nodes is smaller than 0.2, and is considered to be negligible. No smooth decrease of the correlation is observed.

For the correlations between the noise evaluated in position (16,7,7) and cross-sections at the position of the noise source, results are summarized in Fig. 4.7. In this case, the relevant effects are due to the thermal capture cross-section and the thermal removal cross-section.

In addition the correlation between the output taken at the point (16, 7, 7) and the thermal cross-section taken in all the nodes on level 7 is analyzed (see Fig. 4.8). Although the cross-section in the neighborhood of where the noise is evaluated has a significant impact, the strongest correlation is still with the cross-section in the node where the noise source is.

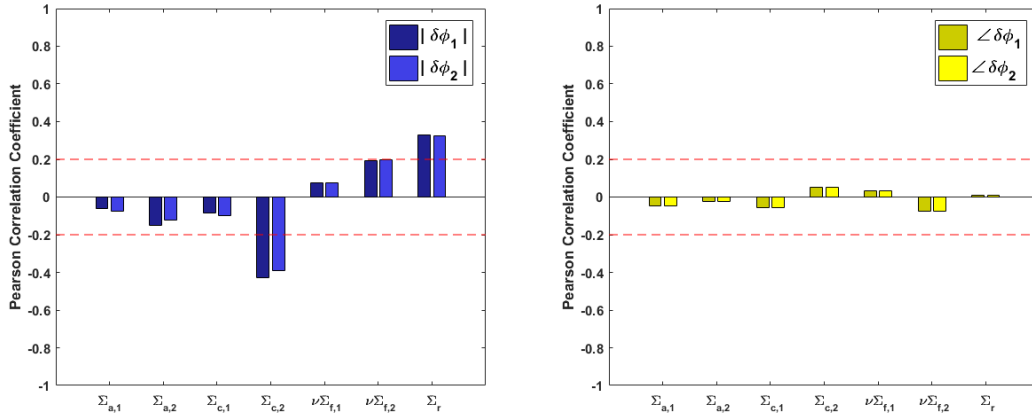


Figure 4.7 Pearson correlation coefficient between each type of cross-section at point (16, 16, 7) where the noise source is and the magnitude of the noise (left), and the phase of the noise (right) at point (16, 7, 7).

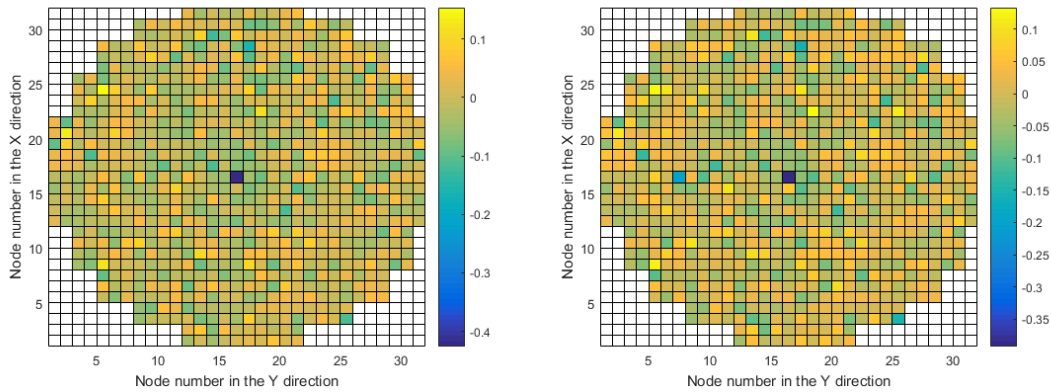


Figure 4.8 The spatial variation of the correlation between the input thermal capture cross sections of the nodes in level 7 and the output the amplitude of the fast and thermal noise at the node (16, 7, 7).

From Fig. 4.6 and Fig. 4.8, it can be concluded that the cross-sections in the node where the source is defined, will play a strong role in the calculation of the magnitude of the noise at both the same node and also other nodes in the core.

### 4.1.3 Pearson correlation coefficient between source strength and noise magnitude over level 7

The Pearson correlation coefficient between the strength of the noise source and the magnitude of the noises of the nodes in level 7 is plotted in Fig. 4.9. The strength of the source has positive, significant correlations to the magnitude of the noise taken in any node on level 7 (the Pearson correlation coefficient is above 0.2 for all the nodes). However, no smooth variation is observed.

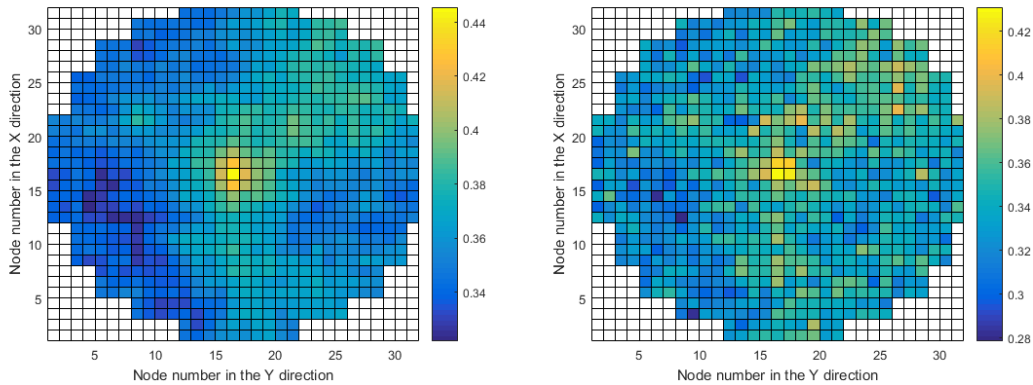


Figure 4.9 The correlation between the strength of the noise source and the magnitude of the fast neutron noise (left) and of the thermal neutron noise (right) at different nodes in level 7.

## 4.2 Sensitivity analysis for the adjoint problem

The input uncertainties for the adjoint calculations are defined according to a uniform probability density function, as for the sensitivity analysis of the forward problem. Thus the adjoint cases that are analyzed, are case G1, G2, H1 and H2 (see Table 2.6).

The adjoint source strength is equal to the one used for the noise source in the thermal absorption cross section. The relationships between the forward and adjoint problem are given by Eqs. (2.45), (2.46) and (3.13)-(3.16). Since the forward noise is evaluated at points (16, 16, 7) and (16, 7, 7), the sources for the adjoint problem are defined in these two points. In fact in the adjoint problem the position of the source corresponds to the position of the forward noise and the position of the adjoint noise corresponds to the position of the forward source.

### 4.2.1 Correlations between the uncertain input parameters and the noise in the same node

For both the G cases and the H cases, the adjoint noise is evaluated at point (16, 16, 7) and point (16, 7, 7). The Pearson correlation coefficient is calculated between the thermal adjoint noise and the cross-sections taken in the same node.

Figure 4.10 shows the results for point (16, 16, 7), in the case G1 (source in the fast group) and in the case G2 (source in the thermal group). The correlations of the adjoint noise with the frequency and the strength of the source are also calculated and included in the plot.

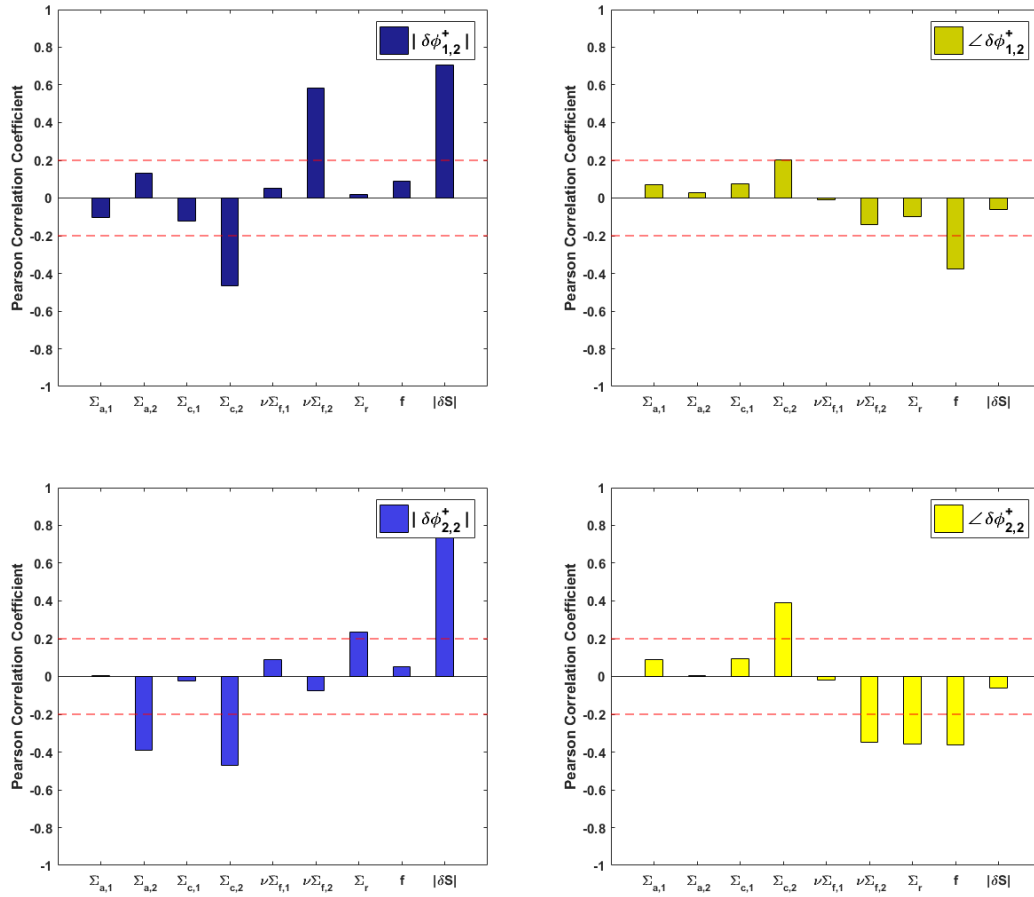


Figure 4.10 The Pearson Correlation Coefficient between the input parameters and (a) the magnitude of the thermal adjoint noise (left figures) and (b) the phase of the thermal adjoint noise (right figures) at the same point (16, 16, 7) in case G1 (top figures) and G2 (bottom figures).

Figure 4.11 shows the correlations between the thermal adjoint noise from the calculations of case G1 and G2, and the input cross sections, when all the quantities are taken at point (16, 7, 7).

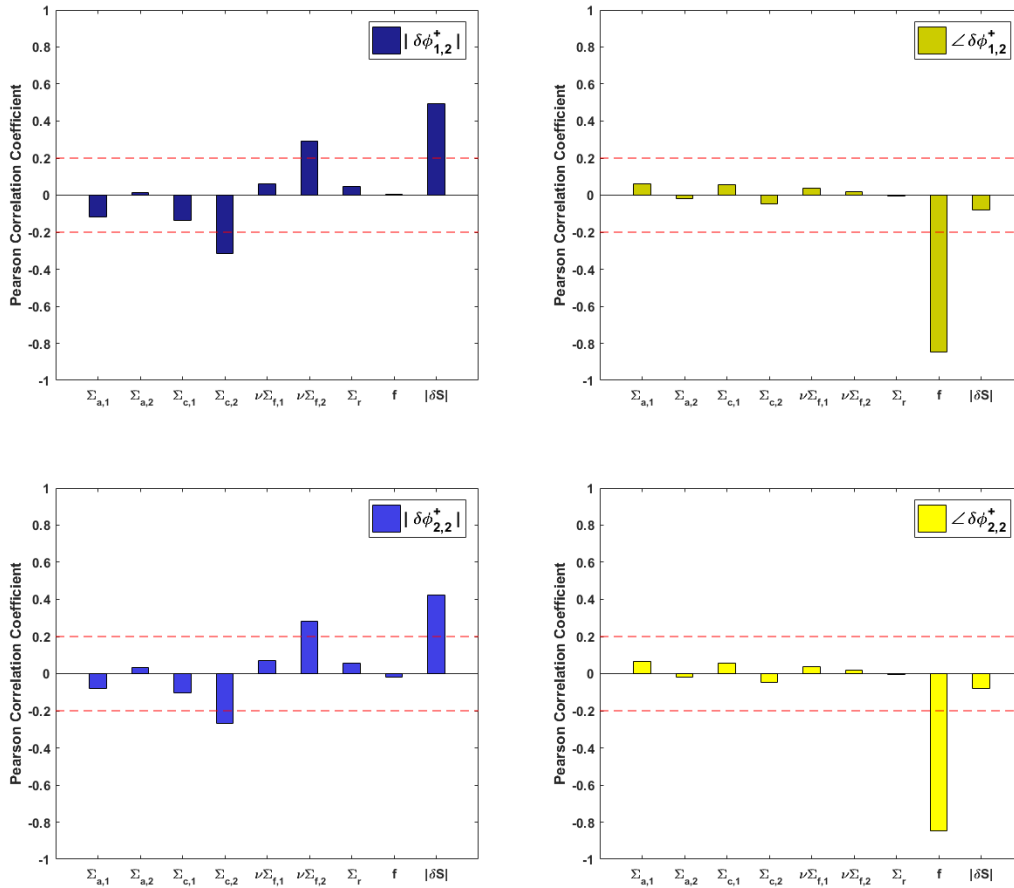


Figure 4.11 The Pearson Correlation Coefficient between the input parameters and (a) the magnitude of the thermal adjoint noise (left figures) and (b) the phase of the thermal adjoint noise (right figures) at the same point (16, 7, 7) in case G1 (top figures) and G2 (bottom figures).

Figure 4.12 and Figure 4.13 are, respectively, for point (16, 16, 7) and point (16, 7, 7), and they show the correlations between the thermal adjoint noise from the calculations of case H1 (source in the fast group) and H2 (source in the thermal group), and the cross sections.

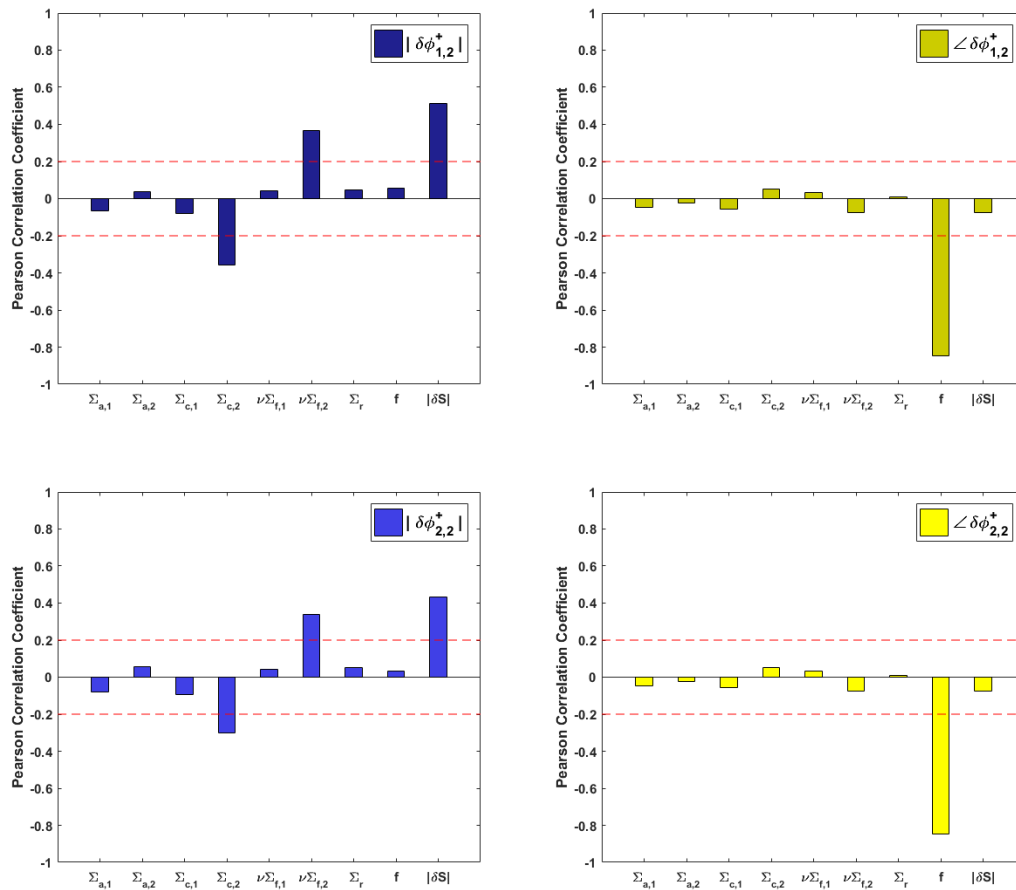


Figure 4.12 The Pearson Correlation Coefficient between the input parameters and (a) the magnitude of the thermal adjoint noise (left figures) and (b) the phase of the thermal adjoint noise (right figures) at the same point (16, 16, 7) in case H1 (top figures) and H2 (bottom figures).

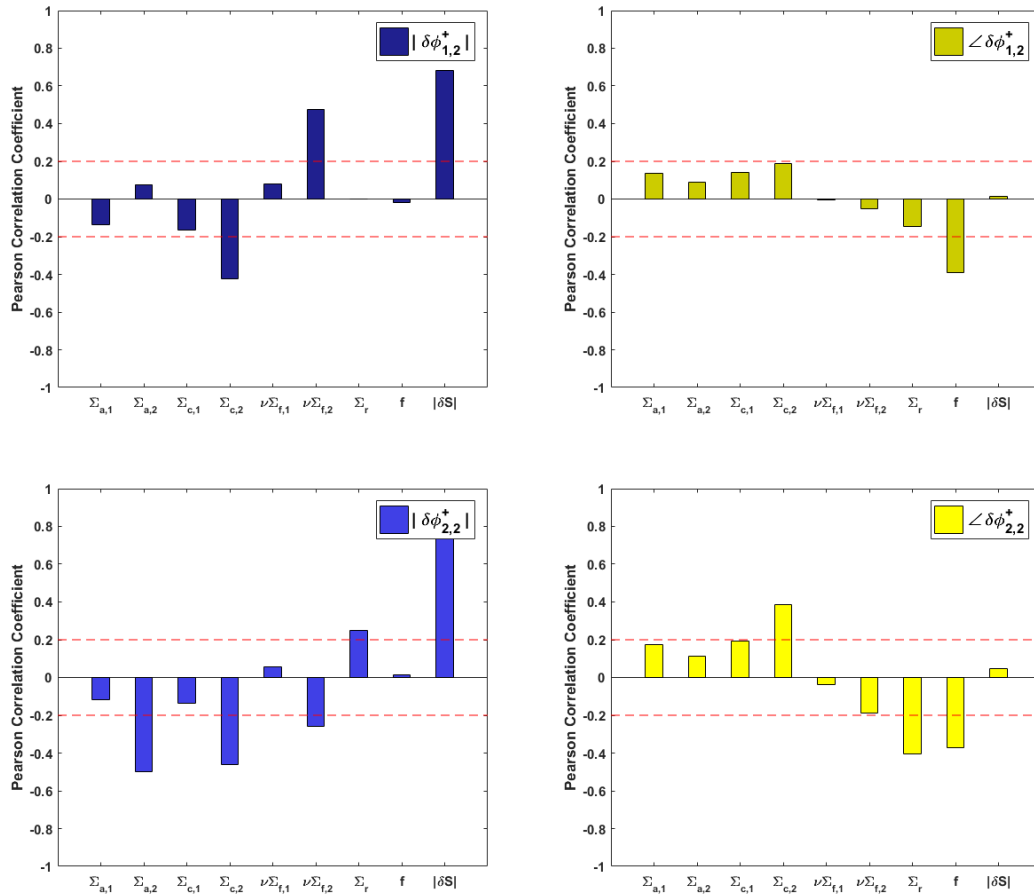


Figure 4.13 The Pearson Correlation Coefficient between the input parameters and (a) the magnitude of the thermal adjoint noise (left figures) and (b) the phase of the thermal adjoint noise at the same point (16, 7, 7) in case H1 (top figures) and H2 (bottom figures).

Figures 4.10 and 4.12 and Figures 4.11 and 4.13 show almost identical results, as the G cases and H cases differ only in the position of the source in the core. Therefore only the results given in Figure 4.10 and 4.11 are commented below.

In Figure 4.10 (plots on the top), the magnitude of the thermal adjoint noise of case G1 (i.e., the source is in the fast group) is affected by the thermal capture cross section according to a negative correlation; and by the thermal fission cross section according to a positive correlation. These two opposite effects result in an insensitive behavior of the magnitude of the thermal adjoint noise to the uncertainty in the thermal absorption cross-section. The other influencing input parameter is the strength of the adjoint noise source, and this plays a major role.

As shown in the plots at the bottom of Figure 4.10, the magnitude of the thermal adjoint noise in case G2 (i.e., the source is defined in the thermal group) is negatively correlated to the thermal capture cross-section (significant effect) and the thermal fission cross-section (slight effect). This results in a more negative correlation with the absorption cross section. A weak correlation is also found with the removal cross-section. Again, the most influential input parameter is the strength of the source.

The frequency shows no correlation to the magnitude of the noises in both cases G1 and G2. Such a behavior is the same as in the forward problem.

The phase of the thermal adjoint noise in case G1 (Figure 4.10, plot on the top-right) is only sensitive to the frequency of the source. For case G2 (Figure 4.10, plot on the bottom-right), there is a positive correlation with the capture cross-section, and a negative correlation with the removal cross-section, with the thermal fission cross-section, and with the frequency. Similarly to the forward problem, the strength of the source has no impact on the phase of the thermal adjoint noise.

The results for cases G1 and G2 at point (16, 7, 7) are given in Fig. 4.11. The magnitude of the thermal adjoint noise in case G1 (plot on the top-left) responds to the change in the cross-sections in a similar manner to what occurs for point (16, 16, 7). However, the correlations are weaker. Such a behavior was also observed for the forward problem.

For the case G2, the correlation between the cross-sections and the magnitude of the thermal adjoint noise are different for point (16, 16, 7) and point (16, 7, 7). As shown in the plot on the bottom-left of Fig. 4.11, the thermal absorption and removal cross-sections are no longer influential at point (16, 7, 7). On the other hand, the thermal fission cross-section has a weak positive effect on the magnitude of the thermal adjoint noise.

For the phase at the point away from the source, i.e. (16, 7, 7), only the frequency has a strong impact.

#### 4.2.2 Pearson correlation coefficient between input parameters and adjoint noise from different nodes

Similarly to the forward problem, the correlations between the cross sections taken in one node and the adjoint noise evaluated in a different node are investigated.

The analysis is performed for both G cases and H cases (Table 2.6). The objective is to evaluate how the adjoint noise at the position of the noise source is influenced by the cross-sections of another node; and how the adjoint noise at a point away from the source is influenced by cross-sections at the location of the source.

Figures 4.14 and 4.15 summarize the results for the G cases. In Fig. 4.14 the cross-section data are taken at point (16, 7, 7) and the thermal adjoint noise is taken at point (16, 16, 7). In Fig. 4.15, it is the opposite: the cross-section data are taken at (16, 16, 7) and the thermal adjoint noise is taken at (16, 7, 7).

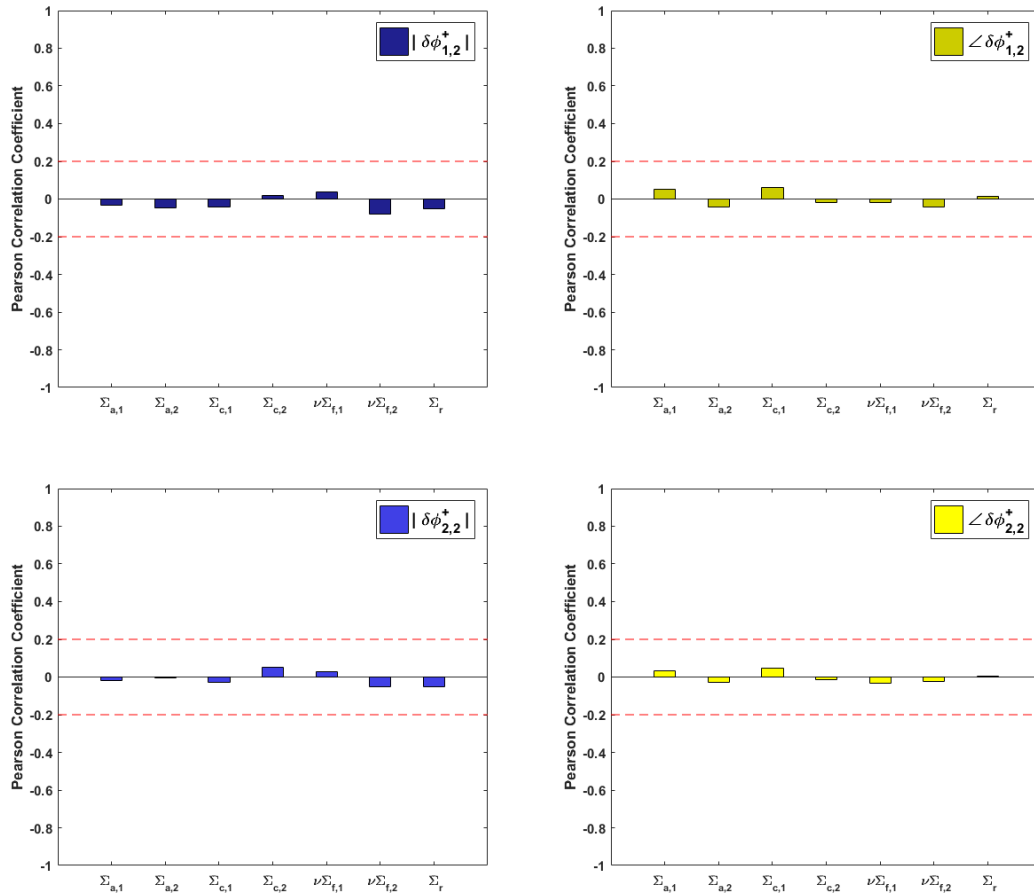


Figure 4.14 Pearson correlation coefficient between cross-sections at point (16, 7, 7) and (a) magnitude of the thermal adjoint noises (left figures) and (b) phase (right figures) at point (16, 16, 7) using the data from cases G1 (top figures) and G2 (bottom figures).

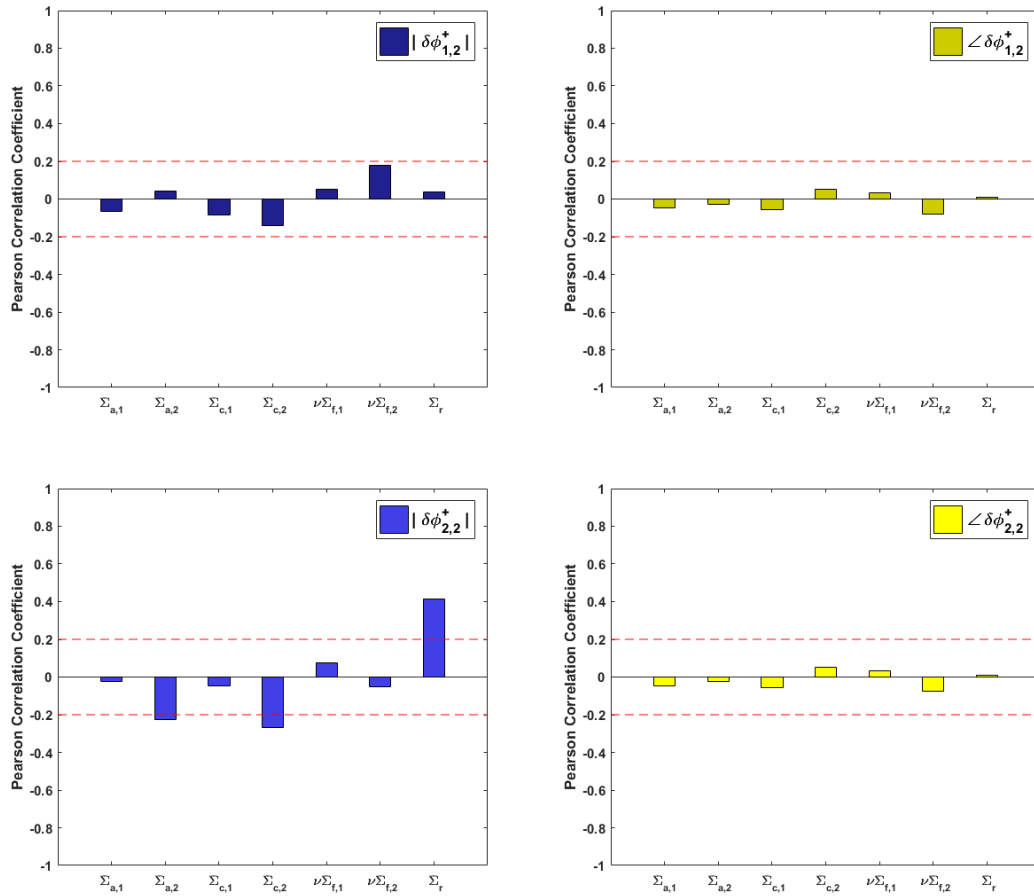


Figure 4.15 Pearson correlation coefficient between cross-sections at point (16, 16, 7) and (a) magnitude of the thermal adjoint noises (left figures) and (b) phase (right figures) at point (16, 7, 7) using the data from cases G1 (top figures) and G2 (bottom figures).

Figures 4.16 and 4.17 are referred to the H cases, where the source is located at (16, 7, 7). In Fig. 4.16 the cross-section data are taken at (16, 16, 7) and the thermal adjoint noise is taken at (16, 7, 7). In Fig. 4.17 the cross-section data are taken at (16, 7, 7) and the thermal adjoint noise is taken from point (16, 16, 7).

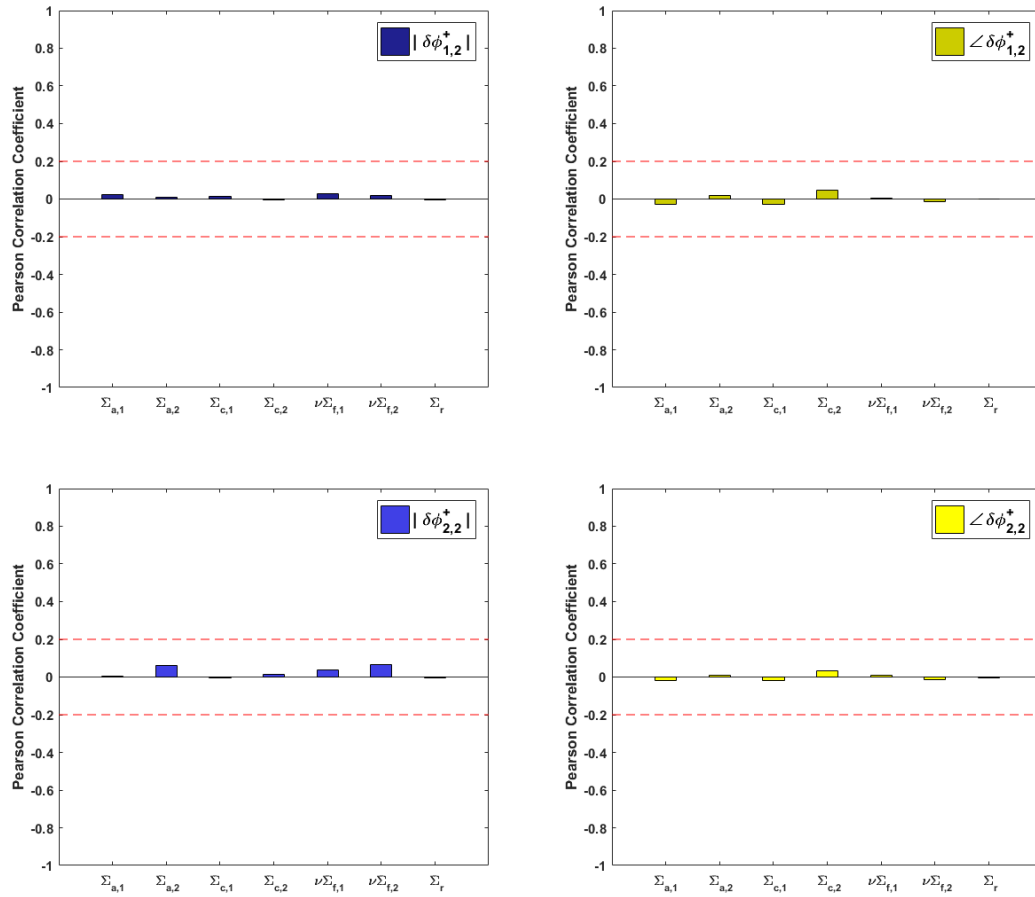


Figure 4.16 Pearson correlation coefficient between cross-sections at point (16, 16, 7) and (a) magnitude of the thermal adjoint noises (left figures) and (b) phase (right figures) at point (16, 7, 7) using the data from cases H1 (top figures) and H2 (bottom figures).

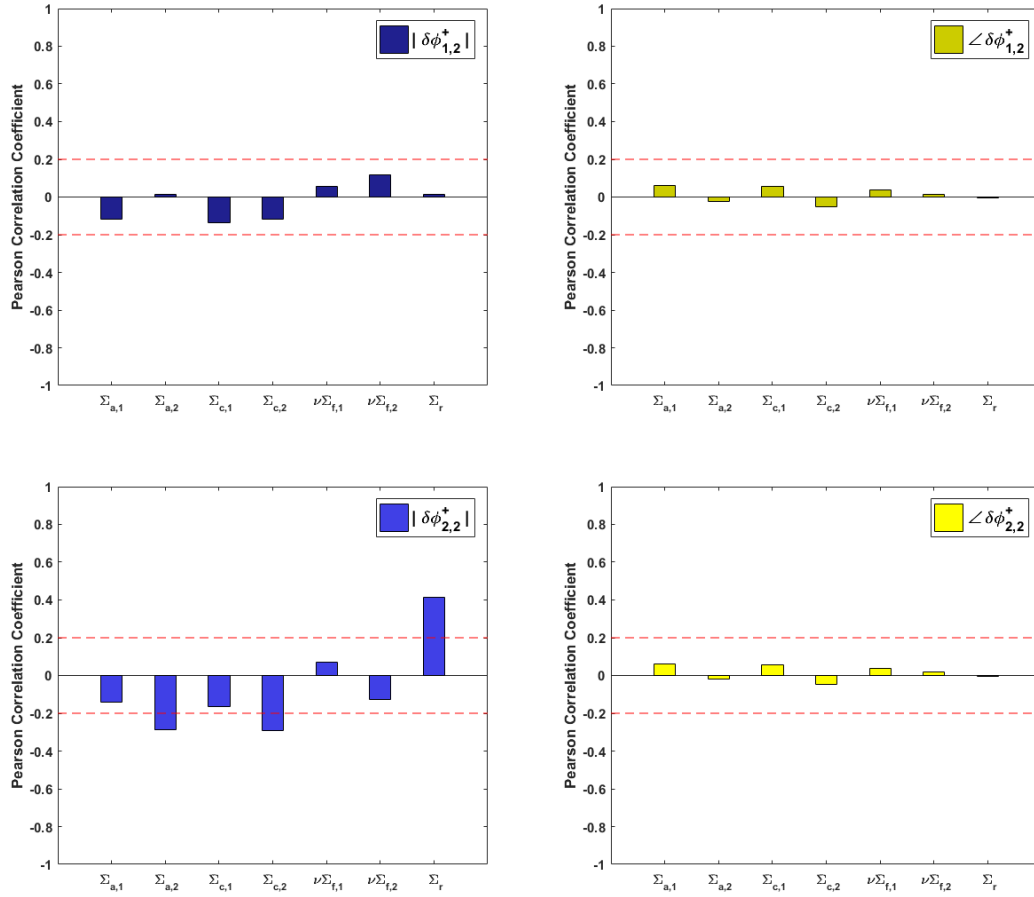


Figure 4.17 Pearson correlation coefficient between cross-sections at point (16, 7, 7) and (a) magnitude of the thermal adjoint noises (left figures) and (b) phase (right figures) at point (16, 16, 7) using the data from cases H1 (top figures) and H2 (bottom figures).

From Figs. 4.14 and 4.16, it can be concluded that the amplitude and phase of the thermal adjoint noise at the location of the source are not affected by the cross-sections in other nodes.

Figures 4.15 and 4.17 show that, when the source is defined in the thermal group, the magnitude of the thermal adjoint noise at a point away from the source, is slightly influenced by some of the cross-sections at the node where the source is placed. These influences are due to a weak negative correlation with the thermal capture cross-sections (and with the thermal absorption cross-section too), and to a positive correlation with the removal cross-section. Again, the phase is not affected by the cross-sections.

In the forward problem, the noise evaluated at point (16, 7, 7), far from the source, is not influenced by the cross-sections at the same point (except a weak effect of the removal cross-section), but rather by the cross-sections at the point where the source is (see Figs. 4.3 and 4.7). The adjoint problem equivalent to this forward problem corresponds to the H cases, and the relative results are given in Fig. 4.12 and 4.17. In these adjoint calculations, the source is defined in (16, 7, 7) and the adjoint noise is

evaluated at point (16, 16, 7). In Fig. 4.12 the adjoint noise at (16, 16, 7), in the H cases, is negatively correlated to the thermal capture cross-section and positively correlated to the thermal fission cross-section, being the cross sections taken at (16, 16, 7). In Fig. 4.17, a different behavior is observed with respect to the one from Fig. 4.12. The cross sections are taken at (16, 7, 7) where the adjoint source is defined, and the thermal absorption and thermal capture cross-sections have a negative correlation with the magnitude of the thermal adjoint noise of case H2 (see the bottom-left plot in Fig. 4.17). In addition, the removal cross section has a positive correlation with the magnitude of the thermal adjoint noise of case H2. The thermal fission cross-section is important in Fig. 4.12, but it is negligible in Fig. 4.17. The same kind of behavior can also be observed in the G cases. Thus the adjoint noise evaluated at a point away from the source may be affected by the cross-sections over the nodes in the core, in different ways.

#### 4.2.3 Pearson correlation coefficient between the source frequency and the phase of the adjoint noise over level 7

In the forward case, the correlation between the source frequency and the phase of both the thermal and fast noise increases in absolute terms, with increasing distance from the source. In the adjoint calculations, a similar phenomenon is observed.

In the adjoint problem an adjoint source is given in a fixed location and the adjoint noise is evaluated in the different points of the core. This corresponds to a forward problem where the noise source is moved in the core, while the noise response is measured in the fixed position of the adjoint source.

The G cases, which have the adjoint noise source defined in point (16, 16, 7), are considered. The analysis of the correlation between the source frequency and the thermal adjoint noise over the entire level 7 is shown in Fig. 4.18. An increase in the absolute value of the Pearson correlation coefficient between the frequency and the thermal adjoint noise is estimated as one moves away from the adjoint source. This smooth increasing variation is similar to the results obtained from the forward cases.

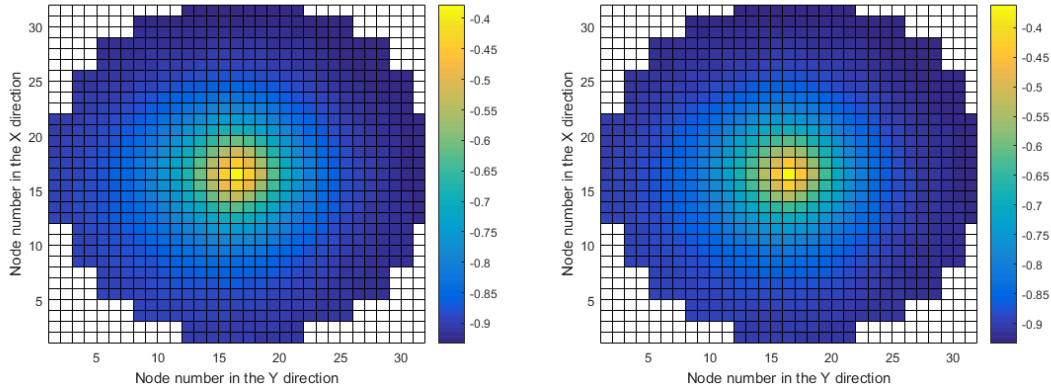


Figure 4.18 Radial dependence of the correlation between the frequency and the phase of the thermal adjoint noise for case G1 (left) and for case G2 (right).

### 4.3 Comparison between the forward and adjoint calculations

The comparison between the results of the forward and adjoint calculations points out that:

1. In both types of calculations, the most significant correlations between cross-sections and noise taken in the same node, are given at the location of the noise source.
2. In both types of calculations, the noise at the point where the source is defined, is only influenced by the cross-sections taken in the same node, while the effect of the cross-sections from other nodes is negligible.
3. In the forward calculations, the noise at other points than the source location, is affected by the cross-sections associated to the location of the source, and this is also observed for the adjoint calculations from the cases G2 and H2.

According to Eqs. (2.44) and (2.45), the sensitivity analysis for the adjoint problem can be compared with the sensitivity analysis for the forward problem as follows.

In the forward problem, the noise evaluated in the position of the source is influenced only by the cross-sections in the same node (see Figs. 4.2 and 4.5). In the corresponding adjoint problem, a similar outcome is obtained (see Figs. 4.10 and 4.14). However, there are differences in the correlations calculated between the cross-sections and the magnitude of the noise taken at the same point (16, 16, 7) where the source is. The comparison between Fig. 4.2 (the forward case) and Fig. 4.10 (the adjoint case), shows that the correlation between the thermal fission cross-section and the thermal adjoint noise of case G1 (which corresponds to the fast forward noise) is found to be stronger than the one in the forward case. The removal cross-section

has positive correlation with the fast forward noise, while it has no impact on the thermal adjoint noise of case G1. In the forward and adjoint calculations, the influence from the strength of the noise source is also stronger.

## 5 Summary and conclusions

This thesis work provides an investigation of the effect of possible input uncertainties on reactor noise calculations by making use of the neutronic tool CORE SIM and a statistical methodology for input uncertainty propagation to the code outputs. Both forward and adjoint problems are considered. The uncertain input parameters included in the study, are the static neutron macroscopic cross-sections, and the strength and frequency of the neutron noise source. These input uncertainties are assumed to be uniformly or normally distributed.

The core is discretized into a large number of nodes and the calculations are made. Two points are chosen where the forward noise is evaluated. The first point is the position where the source is located at, the second point is a position away from the source. Adjoint calculations corresponding to the forward problem are also performed. Using the input and output samples, the sensitivity analysis is carried out.

From the uncertainty analysis, the distribution of the calculated forward noise is close to a normal distribution regardless of how the uncertain input parameters are distributed. However, the distribution of the input parameters still has some influence on the results as the distributions of the outputs show a more peaked behavior when input normal distributions are used. Furthermore, the phase of the forward noise at the point away from the source shows a flattened distribution and this is due to the dependency on the frequency. A similar general behavior for the adjoint calculations is also observed.

From the sensitivity analysis of the forward problem, it is seen that only the macroscopic cross-sections in the thermal group and the removal cross-section will influence noise calculations. The magnitude of the noise at the point where the source is located at, will only be impacted by the cross-sections of the same node. However, the noise located at a position away from the source will be influenced by the cross-sections in the node where the source is. The phase in the node where the source is will be influenced by both the static macroscopic cross-sections and the frequency. The phase at other nodes however, will only be affected by the frequency. The behavior of the corresponding adjoint calculations in general are the same as the forward calculations, but differences still exist as one would expect as the structure of the equation solved are changed.

This project represents the first effort to assess the impact of input uncertainties on reactor noise calculations. Future studies may be conducted on different aspects. As mentioned above, the input uncertainties were assumed normally or uniformly distributed. However, more realistic quantification of the uncertainties in the cross-sections can be based on experimental data. Although diffusion coefficients were not included in this work, they may be a source of uncertainty that cannot be disregarded. About the sensitivity analysis, further work is needed for a better understanding of the interplay between input parameters, uncertainties and neutron noise. For instance, a closer analysis of the behavior of the noise phase may be of particular interest.



# Reference

- [1] World Nuclear Association, Nuclear Power in the World Today, 2017  
<http://www.world-nuclear.org/information-library/current-and-future-generation/nuclear-power-in-the-world.aspx> (accessed on May 9 2017).
- [2] Glasstone S, Sesonske A. Nuclear reactor engineering: reactor systems engineering [M]. Springer Science & Business Media, 2012.
- [3] Pázsit I, Kuang Z F, Prinja A K. A unified theory of zero power and power reactor noise via backward master equations [J]. Annals of Nuclear Energy, 2002, 29(2): 169-192.
- [4] Demazière C, Andhill G. Identification and localization of absorbers of variable strength in nuclear reactors[J]. Annals of Nuclear Energy, 2005, 32(8): 812-842.
- [5] Arzhanov V, Pázsit I. Diagnostics of core barrel vibrations by in-core and ex-core neutron noise[J]. Progress in Nuclear Energy, 2003, 43(1): 151-158.
- [6] Demazière C, Pázsit I. Development of a method for measuring the moderator temperature coefficient by noise analysis and its experimental verification in Ringhals-2[J]. Nuclear science and engineering, 2004, 148(1): 1-29.
- [7] Demazière C, Pázsit I. Power reactor noise, lecture notes[C]//Workshop on Neutron Fluctuations, Reactor Noise, and their Applications in Nuclear Reactors, International Centre for Theoretical Physics, Trieste, Italy. 2008.
- [8] Demazière C. CORE SIM: a multi-purpose neutronic tool for research and education [J]. Annals of Nuclear Energy, 2011, 38(12): 2698-2718.
- [9] Demazière C. Development of a 2-D 2-group neutron noise simulator[J]. Annals of Nuclear Energy, 2004, 31(6): 647-680.
- [10] Glaeser H. GRS method for uncertainty and sensitivity evaluation of code results and applications[J]. Science and Technology of Nuclear Installations, 2008, 2008.
- [11] Wilks S S. Determination of sample sizes for setting tolerance limits [J]. The Annals of Mathematical Statistics, 1941, 12(1): 91-96.
- [12] Engineering Statistics Handbook, 1.3.5.11-Measures of Skewness and Kurtosis, <http://www.itl.nist.gov/div898/handbook/eda/section3/eda35b.htm> (accessed on May 15 2017).
- [13] Fieller E C, Hartley H O, Pearson E S. Tests for rank correlation coefficients. I[J]. Biometrika, 1957, 44(3/4): 470-481.
- [14] Gibbons J D, Chakraborti S. Nonparametric statistical inference[M]. Springer Berlin Heidelberg, 2011.
- [15] Fisher R A. Statistical methods for research workers [M]. Genesis Publishing Pvt Ltd, 1925.